clinical factors influencing hepatic complications. In clinical settings, it is important to predict the onset of severe liver injury associated with AN, which could be potentially life-threatening, and therefore it was anticipated that the information obtained from the present study would be of value to clinicians in assessing the risk of developing this serious complication.

METHODS

Study population

THIS RETROSPECTIVE OBSERVATION study was conducted between January 2010 and December 2011 at the Department of Gastroenterology and Department of Neuropsychiatry, Yamagata University Hospital. During this 2-year period, a total of 37 patients were admitted under a diagnosis of AN. These patients comprised both newly referred patients and established outpatients with exacerbation. There were also first admissions and repeat admissions due to deterioration of the patients' condition. The diagnosis of AN was made by a psychiatrist in accordance with the criteria of the Diagnostic and Statistical Manual of Mental Disorders, 4th edition (DSM-IV) on the basis of information obtained by interview from the patients and their families. The exclusion criteria were: (i) a history of hepatic disease, (ii) established infection with hepatitis viruses (HBV or HCV), (iii) drug abuse, (iv) excessive alcohol intake, and (v) presence of autoimmune liver disease. Especially for patients with highly elevated ALT, imaging studies (both ultrasound and dynamic CT scan) were performed to exclude other hepatobiliary diseases.

Study design

Clinical physiological parameters such as age, gender, BMI, body temperature, pulse rate, and blood pressure were evaluated, as well as routine laboratory data obtained on admission. Routine laboratory data included a complete blood cell count (CBC), hepatobiliary enzyme levels, renal function and blood sugar (BS) levels. The enrolled patients were subjected to subgroup analysis and categorized into three groups: (i) normal ALT defined as a serum ALT level of <42 IU/L, (ii) moderately elevated ALT defined as a serum ALT level between 42 IU/L and <840 IU/L (20 times above the institutional upper normal limit), and (iii) highly elevated ALT defined as a serum ALT level of >840 IU/L.

Statistical analysis

The above three subgroups were evaluated statistically by analysis of variance (ANOVA). If a significant difference was found, multiple comparisons (post hoc test) were performed with Tukey–Kramer and Steel–Dwass test. The risk related to elevated ALT was analyzed by univariate and multivariate logistic regression. The results of logistic regression analysis were expressed as odds ratio with 95% confidence interval. Differences after these modifications were considered significant at $P < 0.05$. Analyses were performed by using Excel Statistics (2010, Social Survey Research Information, Tokyo, Japan).

RESULTS

Patient features

THE BACKGROUNDS OF the 37 enrolled patients are listed in Table 1. The ages of the patients ranged from 12 to 67 years (median age 24 years), and all were lean females with a mean BMI on admission of 13 kg/m². The serum ALT level ranged widely from 11 to 2321 IU/L, with a median of 27 IU/L. Besides liver injury, physiological and laboratory abnormalities frequently associated with AN, such as bradycardia, hypothermia, hypotension, anemia, leukopenia, thrombocytopenia, hyponatremia, hypokalemia, and hypoglycemia were present in some of the enrolled patients.

Comparison of each clinical parameter according to the ALT level

Elevated liver enzyme (serum ALT level ≥42 IU/L) was observed in 13 (35%) of the 37 cases. Highly elevated ALT was evident in four cases (11%), the median ALT level being 1986.5 IU/L. Patients in the moderately elevated ALT group accounted for 24% of the subjects overall (9/37), and the median ALT level was 71 IU/L. The median serum ALT level in the normal ALT group was 20.5 IU/L. The clinical parameters in these three groups are detailed in Table 2. Among the clinical parameters evaluated, body temperature, pulse rate, blood urea nitrogen (BUN), BUN/creatinine ratio, BS, and platelet count differed significantly among the groups ($P < 0.05$). These six parameters were further analyzed statistically, and this revealed that both BUN and the BUN/creatinine ratio were significantly higher in the high ALT group than in the normal ALT ($P < 0.05$) and moderate ALT ($P < 0.05$) groups, respectively (Fig. 1). Body temperature, BS and platelet count were

© 2013 The Japan Society of Hepatology

Table 1 Characteristics of study population ($n = 37$)

Parameter	Mean ± SD	Range
Age (years)[†]	24	12–67
BMI (kg/m^2)	13.0 ± 2.2	9.5–17.9
Body temperature (°C)	36.5 ± 0.7	34.5–38.0
Pulse rate (bpm)	72.1 ± 19.8	46–111
Systolic blood pressure (mmHg)	95.8 ± 18.0	67–153
Diastolic blood pressure (mmHg)	63.2 ± 15.3	33–101
Albumin (g/dL)	4.4 ± 0.9	2.6–5.7
Total bilirubin (mg/dL)[†]	0.9	0.2–7.3
AST (IU/L)[†]	29	12–2628
ALT (IU/L)[†]	27	11–2321
BUN (mg/dL)	19.8 ± 11.3	4–47
Creatinine (mg/dL)[†]	0.66	0.16–1.57
BUN/creatinine (ratio)[†]	24.3	8–104.4
Na (mEq/L)[†]	140	121–146
K (mEq/L)	3.7 ± 0.6	2.4–5.1
Cl (mEq/L)	99.8 ± 6.8	76–110
Blood sugar (mg/dL)[†]	81	12–150
White blood cells (/μL)	5132.9 ± 2564.7	1 820–15 600
Hemoglobin (g/dL)	12.6 ± 2.0	5.7–16.5
Platelet count (/μL)	23.6 ± 9.2	8.1–41.1

[†]Median.
ALT, alanine aminotransferase; AST, aspartate aminotransferase; BMI, body mass index; BUN, blood urea nitrogen; SD, standard deviation.

Table 2 Comparison of each clinical parameter according to the alanine aminotransferase (ALT) level

Parameter	Highly elevated ALT group (ALT ≥ 840) $n = 4$	Moderately elevated ALT group (840 > ALT ≥ 42) $n = 9$	Normal ALT group (ALT < 42) $n = 24$	P-value
Age (years); median [range]	17 [16–31]	29 [13–50]	22 [12–67]	0.495
BMI (kg/m^2); mean ± SD	10.7 ± 1.1	13.4 ± 3.0	13.3 ± 1.8	0.070
Body temperature (°C); mean ± SD	35.3 ± 0.9	36.8 ± 0.5	36.7 ± 0.7	<0.05
Pulse rate (bpm); mean ± SD	50.5 ± 12.2	67.7 ± 15.7	75.9 ± 20.1	<0.05
Systolic blood pressure (mmHg); mean ± SD	92.3 ± 12.1	97.7 ± 11.6	95.7 ± 20.9	0.890
Albumin (g/dL); mean ± SD	4.4 ± 0.6	3.9 ± 1.0	4.6 ± 0.8	0.110
AST (IU/L); median [range]	2249.5 [1684–2628]	68 [39–512]	22 [12–53]	<0.05
ALT (IU/L); median [range]	986.5 [871–2321]	71 [48–215]	20.5 [11–36]	<0.05
BUN (mg/dL); mean ± SD	41.0 ± 6.1	17.4 ± 9.9	17.1 ± 8.6	<0.05
Creatinine (mg/dL); median [range]	0.64 [0.45–0.67]	0.56 [0.35–0.7]	0.71 [0.16–1.57]	0.062
BUN/creatinine; median [range] (ratio)	63.6 [53.2–104.4]	28.3 [11.6–56.9]	19.4 [8–68.6]	<0.05
Na (mEq/L); mean ± SD	141.0 ± 5.0	138.2 ± 3.6	138.4 ± 5.3	0.592
K (mEq/L); mean ± SD	3.7 ± 0.3	3.7 ± 0.6	3.7 ± 0.7	0.998
Cl (mEq/L); mean ± SD	102.3 ± 7.4	100.3 ± 4.0	99.3 ± 7.6	0.89
Blood sugar (mg/dL); median [range]	26 [12–46]	80 [57–109]	84.5 [62–159]	<0.05
White blood cells (/μL) mean ± SD;	6067.5 ± 2880.3	4503 ± 1749.3	5213.3 ± 2799.2	0.591
Hemoglobin (g/dL); mean ± SD	12.1 ± 4.3	12.1 ± 3.9	12.8 ± 1.7	0.706
Platelet count (/μL); mean ± SD	10.4 ± 2.1	24.9 ± 7.9	25.3 ± 8.7	<0.05

AST, aspartate aminotransferase; BMI, body mass index; BUN, blood urea nitrogen; SD, standard deviation.
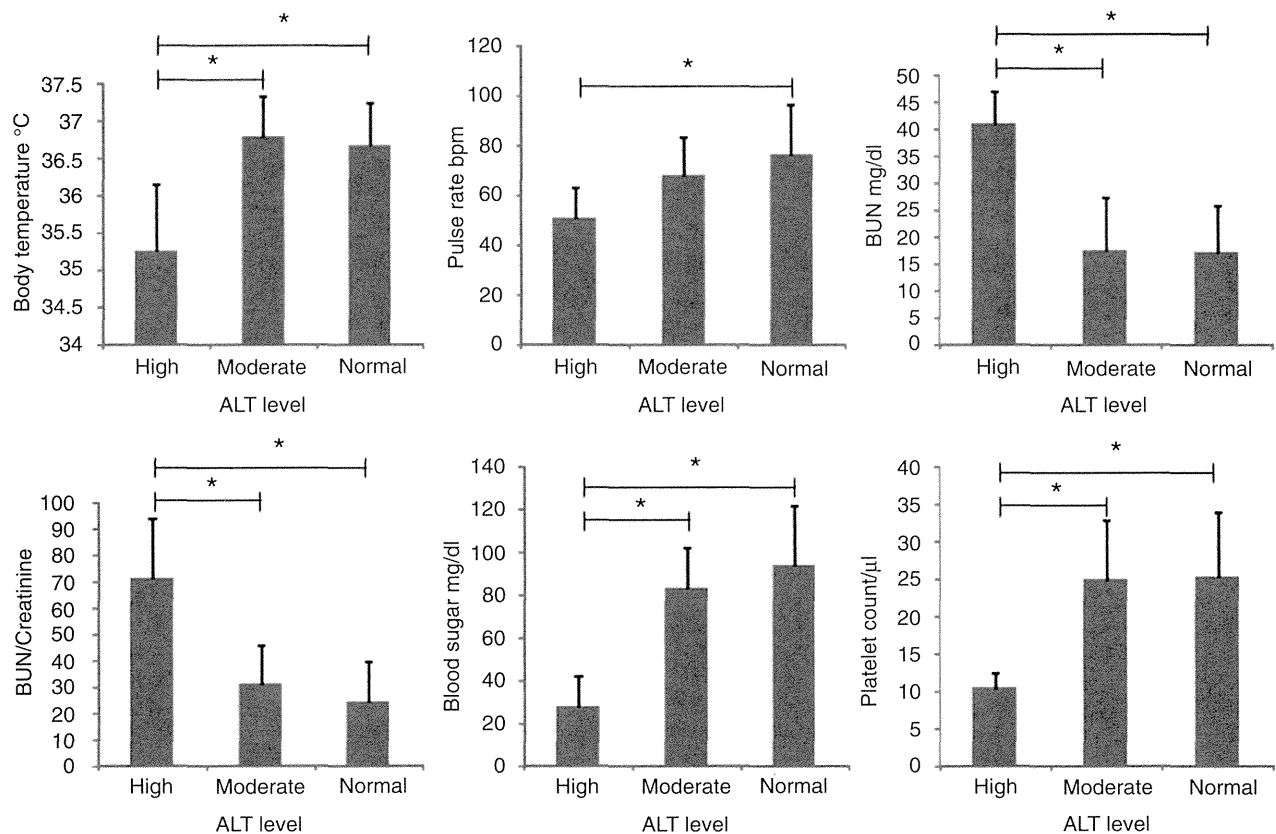
Figure 1 Statistically significant clinical parameters (body mass index [BMI], pulse rate, blood urea nitrogen [BUN], BUN/creatinine ratio, blood sugar, platelets count) among the three groups divided according to the severity of liver injury. Multiple comparisons (post hoc test) were performed with Tukey–Kramer and Steel–Dwass test. *P < 0.05.

significantly lower in the high ALT group than in the normal ALT (P < 0.05) and moderate ALT (P < 0.05) groups. Pulse rate in the high ALT group was significantly decreased than in the normal ALT group (P < 0.05), but the difference between the high ALT and moderate ALT groups was not significant.

Risk factors related to elevated ALT levels in patients with AN

Among the six parameters (body temperature, pulse rate, BUN, BUN/creatinine, BS, platelet count) initially demonstrating significant differences among the three groups, risk factors relating to elevated ALT levels were examined. BUN/creatinine and BS were significantly associated with the incidence of elevated ALT by univariate analyses (Table 3). In further analysis with multiple logistic regression, there was not a significant association between the six parameters (body temperature, pulse rate, BUN, BUN/creatinine, BS, platelet count).

However, there was a trend with BUN/creatinine (odds ratio [OR] = 1.051; 95% confidence interval [CI]; 0.999–1.105, P = 0.054) and BS (OR = 0.967; 95% CI; 0.933–1.002, P = 0.066 (Table 3).

DISCUSSION

WE FOUND THAT AN patients with highly elevated ALT had a significantly high BUN level and BUN/creatinine ratio, and a low body temperature, low blood sugar level, and low platelet count. Moreover, BUN/creatinine and BS had trends associated with the incidence of elevated ALT by multivariate analyses.

Clinical parameters in patients with AN demonstrating liver injury have been reported previously, especially the relationship between elevation of serum liver enzyme levels and low BMI.[6,7] However, in the present study, we found no significant correlation of serum liver

Table 3 Multiple logistic regression analysis related to elevated alanine aminotransferase (ALT) levels in anorexia nervosa (AN) patients

	Univariate		Multivariate	
	OR (95% CI)	*P*-value	OR (95% CI)	*P*-value
BUN/Creatinine (ratio)	1.051 (1.008–1.096)	0.019	1.051 (0.999–1.105)	0.054
Blood sugar (mg/dL)	0.962 (0.930–0.995)	0.025	0.967 (0.933–1.002)	0.066
Body temperature (°C)	0.509 (0.192–1.347)	0.174		
Pulse rates (bpm)	0.958 (0.916–1.002)	0.061		
BUN (mg/dL)	1.064 (0.997–1.135)	0.062		
Platelet count (/μL)	0.939 (0.866–1.019)	0.131		

Stepwise method was used to select the variables in multiple logistic regression analysis.
BUN, blood urea nitrogen; CI, confidence interval; OR, odds ratio.

enzyme levels with BMI. We speculate that this may have been attributable to the inclusion criteria we used for our AN patients. The present study recruited only AN patients who required hospitalization, so our study patients tended to have lower BMI values than outpatient studies, thus possibly masking any statistically significant differences.

Among several clinical parameters, we found that the serum BUN level and BUN/creatinine ratio were significantly high in the high ALT group. We speculate that this phenomenon could have been attributable to the presence of severe dehydration in this group, where a high BUN level and a high BUN/creatinine ratio (so-called "hypoxic hepatitis") were also observed. This is in accord with the fact that even patients with severe liver injury usually recover after conservative treatment such as drip infusion or bed rest, as seen in cases of hypoxic hepatitis due to circulatory failure occasionally encountered in various clinical settings.

We also observed that the high ALT group had significantly lower values of pulse rate. It seems paradoxical that AN patients with severe liver injury often have bradycardia despite the presence of severe dehydration. We speculate that this phenomenon may be due to the fact that patients with AN usually have hypertonic parasympathetic nervous conditions and hypotonic sympathetic nervous conditions, which lead to failure to respond to the stimulation of the sympathetic nervous system resulting from dehydration.[8] Also, among our AN patients in the high ALT group, hypoglycemia (median value as low as 26 mg/dL) was observed in four, and this led to consciousness disturbance in two. Up to now, there have been no convincing explanations for the hypoglycemia and liver injury associated with AN, although hypoglycemia could affect the systemic circu-

lation, in turn influencing the hepatic circulation and resulting in liver injury. In fact, it has been reported that patients with hypoxic hepatitis are often complicated by hypoglycemia.[9]

In patients with AN, various complications known as "refeeding syndrome" can occur after initiation of food intake or hyperalimentation on admission and hypoglycemia is one of its symptoms.[10] Although some reports have described the presence of liver injury during hypoglycemia in refeeding syndrome,[11,12] its precise mechanism remains unknown.

Our present findings suggested a close relationship of dehydration in the pathogenesis of elevated liver enzyme in AN, with features clinically reminiscent of hypoxic hepatitis. However, we were not able to exclude the opposite possibility that high BUN and BUN/ creatinine ratio could be caused by elevated ALTs. Unfortunately this is the limitation of this retrospective study. Our study was also limited in that it did not evaluate liver pathology. Hepatic histological findings in AN with liver insufficiency include centrilobular lesions with fibrosis or atrophy, hepatocytes swelling, glycogen depletion, and ceroid pigmentation.[13] Since almost all patients with AN are young females, who often have accompanying mood disorder and/or obsessive-compulsive disorder,[14] and liver injury rapidly improves after hospitalization,[15] invasive procedures such as liver biopsy are rarely performed at an early stage after admission when patients are psychiatrically unstable. Accordingly, future studies will need to evaluate liver histology or use an appropriate animal model.

In conclusion, the present study has demonstrated that AN patients with severe liver injury have significantly increased in the serum BUN level and BUN/ creatinine ratio. This could account for failure of the

hepatic circulation due to severe dehydration based on malnutrition, being a potentially important factor in the development of severe liver injury in AN patients, mimicking hypoxic hepatitis. These factors offer an interesting insight into the pathogenesis of AN.

ACKNOWLEDGMENT

REFERENCES

1 Kuboki T, Nomura S, Ide M, Suematsu H, Araki S. Epidemiological data on anorexia nervosa in Japan. *Psychiatry Res* 1996; **62**: 11–16.

2 Fong HF, DiVasta AD, DiFabio D, Ringelheim J, Jonas MM, Gordon CM. Prevalence and predictors of abnormal liver enzymes in young women with anorexia nervosa. *J Pediatr* 2008; **153**: 247–53.

3 De Caprio C, Alfano A, Senatore I, Zarrella L, Pasanisi F, Contaldo F. Severe acute liver damage in anorexia nervosa: two case reports. *Nutrition* 2006; **22**: 572–5.

4 Furuta S, Ozawa Y, Maejima K et al. Anorexia nervosa with severe liver dysfunction and subsequent critical complications. *Intern Med* 1999; **38**: 575–9.

5 Dowman J, Arulraj R, Chesner I. Recurrent acute hepatic dysfunction in severe anorexia nervosa. *Int J Eat Disord* 2010; **43**: 770–2.

6 Tsukamoto M, Tanaka A, Arai M et al. Hepatocellular injuries observed in patients with an eating disorder prior to nutritional treatment. *Intern Med* 2008; **47**: 1447–50.

7 Ozawa Y, Shimizu T, Shishiba Y. Elevation of serum aminotransferase as a sign of multiorgan-disorders in severely emaciated anorexia nervosa. *Intern Med* 1998; **37**: 32–9.

8 Petretta M, Bonaduce D, Scalfi L et al. Heart rate variability as a measure of autonomic nervous system function in anorexia nervosa. *Clin Cardiol* 1997; **20**: 219–24.

9 Fuhrmann V, Kneidinger N, Herkner H et al. Hypoxic hepatitis: underlying conditions and risk factors for mortality in critically ill patients. *Intensive Care Med* 2009; **35**: 1397–405.

10 Crook MA, Hally V, Panteli JV. The importance of the refeeding syndrome. *Nutrition* 2001; **17**: 632–7.

11 Sakurai-Chin C, Ito N, Taguchi M, Miyakawa M, Takeshita A, Takeuchi Y. Hypoglycemic coma in a patient with anorexia nervosa coincident with acute exacerbation of liver injury induced by oral intake of nutrients. *Intern Med* 2010; **49**: 1553–6.

12 Narayanan V, Gaudiani JL, Harris RH, Mehler PS. Liver function test abnormalities in anorexia nervosa-cause or effect. *Int J Eat Disord* 2010; **43**: 378–81.

13 Rautou P-E, Cazals-Hatem D, Mareau R et al. Acute liver cell damage in patients with anorexia nervosa: a possible role of starvation-induced hepatocyte autophagy. *Gastroenterology* 2008; **135**: 840–8.

14 Salbach-Andrae H, Lenz K, Simmendinger N, Klinkowski N, Lehmkuhl U, Pfeiffer E. Psychiatric comorbidities among female adolescents with anorexia nervosa. *Child Psychiatry Hum Dev* 2008; **39**: 261–72.

15 Giordano F, Arnone S, Santeusanio F, Pampanelli S. Brief elevation of hepatic enzymes due to liver ischemia in anorexia nervosa. *Eat Weight Disord* 2010; **15**: E294–7.

Nrf2 Enhances Cholangiocyte Expansion in Pten-Deficient Livers

Keiko Taguchi,[a,b] Ikuo Hirano,[b] Tohru Itoh,[c] Minoru Tanaka,[c] Atsushi Miyajima,[c] Akira Suzuki,[d] Hozumi Motohashi,[a] Masayuki Yamamoto[b]

Department of Gene Expression Regulation, Institute of Development, Aging and Cancer, Tohoku University, Sendai, Japan[a]; Department of Medical Biochemistry, Tohoku University Graduate School of Medicine, Sendai, Japan[b]; Laboratory of Cell Growth and Differentiation, Institute of Molecular and Cellular Biosciences, The University of Tokyo, Tokyo, Japan[c]; Division of Cancer Genetics, Department of Molecular Genetics, Medical Institute of Bioregulation, Kyushu University, Fukuoka, Japan[d]

Keap1-Nrf2 system plays a central role in the stress response. While Keap1 ubiquitinates Nrf2 for degradation under unstressed conditions, this Keap1 activity is abrogated in response to oxidative or electrophilic stresses, leading to Nrf2 stabilization and coordinated activation of cytoprotective genes. We recently found that nuclear accumulation of Nrf2 is significantly increased by simultaneous deletion of Pten and Keap1, resulting in the stronger activation of Nrf2 target genes. To clarify the impact of the cross talk between the Keap1-Nrf2 and Pten–phosphatidylinositide 3-kinase–Akt pathways on the liver pathophysiology, in this study we have conducted closer analysis of liver-specific *Pten::Keap1* double-mutant mice (Pten::Keap1-Alb mice). The Pten::Keap1-Alb mice were lethal by 1 month after birth and displayed severe hepatomegaly with abnormal expansion of ductal structures comprising cholangiocytes in a Nrf2-dependent manner. Long-term observation of Pten::Keap1-Alb::Nrf2$^{+/-}$ mice revealed that the Nrf2-heterozygous mice survived beyond 1 month but developed polycystic liver fibrosis by 6 months. Gsk3 directing the Keap1-independent degradation of Nrf2 was heavily phosphorylated and consequently inactivated by the double deletion of *Pten* and *Keap1* genes. Thus, liver-specific disruption of *Keap1* and *Pten* augments Nrf2 activity through inactivation of Keap1-dependent and -independent degradation of Nrf2 and establishes the Nrf2-dependent molecular network promoting the hepatomegaly and cholangiocyte expansion.

The Keap1-Nrf2 system is a critical defense mechanism against oxidative and electrophilic stresses (1). Nrf2 (nuclear factor erythroid 2-related factor 2) is a potent transcriptional activator that binds to antioxidant/electrophile-responsive elements (ARE/EpRE) with small Maf (2), leading to the upregulation of cytoprotective genes encoding antioxidant proteins, xenobiotic-detoxifying enzymes, and drug transporters. Keap1 (Kelch-like ECH-associated protein 1) is a cullin 3 (Cul3)-based E3 ubiquitin ligase adaptor that mediates the ubiquitination of Nrf2 in the cytoplasm, promoting the proteasomal degradation of Nrf2 under unstressed conditions. When cells are exposed to oxidative or electrophilic stresses, the cysteine residues of Keap1 are modified, resulting in the attenuation of Nrf2 ubiquitination. The Nrf2 that escapes Keap1-mediated degradation translocates into the nucleus and activates cytoprotective genes, conferring resistance to these stresses (3).

Recent studies have revealed that Nrf2 augments the metabolic reprogramming of cells in the presence of active proliferative signals, particularly the phosphatidylinositide 3-kinase (PI3K)–Akt pathway, through the activation of metabolic genes, resulting in the acceleration of cell proliferation (4, 5). Indeed, in various human cancer cells, Nrf2 is constitutively stabilized through genetic and/or epigenetic factors, promoting the proliferation of these cells (6–8). A similar association between cell proliferation signals and Nrf2 has been observed in *Keap1*-null mice, which exhibit the constitutive stabilization/activation of Nrf2 throughout the body. In *Keap1*-null mice, the cells of certain lineages are more proliferative than those of wild-type mice in an Nrf2-dependent manner. Basal layer keratinocytes in the upper digestive tract grow rapidly and cause obstructive thickening under conditions of defective Keap1 function (9–11). Immature megakaryocytes cultured from *Keap1*-null fetal livers also show rapid proliferation (12). These observations suggested that Nrf2 is a facultative or context-dependent accelerator of proliferation that does not inherently provoke

cell cycle progression but requires proliferative signals to promote cell proliferation (13, 14). However, the molecular mechanisms and pathophysiological consequences of the expansion of Nrf2 function through active proliferative signals remain to be clarified.

Pten (phosphatase and tensin homolog deleted from chromosome 10) is a well-known tumor suppressor gene that counteracts the PI3K-protein kinase B (PKB)-Akt pathway. The functional loss of *Pten* increases Akt phosphorylation, which promotes cell growth, proliferation, and survival through the modulation of protein synthesis and metabolism (15). *PTEN* mutations and deficiencies are often detected in many types of human cancers (16). Approximately 40% of cases of hepatocellular carcinomas show a decrease or an absence of PTEN expression (17). Liver-specific *Pten* knockout mice serve as an animal model of liver carcinogenesis associated with nonalcoholic fatty liver disease (18, 19). These mice spontaneously develop hepatocellular carcinomas and, with less frequency, cholangiocellular carcinomas after they reach 1 year of age. We observed that Pten deficiency significantly augments Nrf2 accumulation in the nucleus (4). Considering that this observation reveals a molecular mechanism linking Nrf2 activation and cell proliferation signals (4), we initiated a study addressing the cross talk between the Keap1-Nrf2 system and the Pten-PI3K-Akt pathway.

To clarify the functional interactions of these pathways in the

liver, we generated $Pten^{flox/flox}$::$Keap1^{flox/flox}$::*Albumin*-Cre (Pten:: Keap1-Alb) mice. $Pten^{flox/flox}$::*Albumin*-Cre (Pten-Alb) mice exhibit steatosis that progresses into tumorigenesis (18), whereas $Keap1^{flox/flox}$::*Albumin*-Cre (Keap1-Alb) mice do not exhibit apparent liver damage or dysfunction (11). Although Pten-Alb and Keap1-Alb mice survived longer, we found that the Pten::Keap1-Alb mice were lethal by 1 month after birth. Surprisingly, the Pten::Keap1-Alb mice displayed severe hepatomegaly, pathological liver enlargement by more than three times compared with normal average liver size, with abnormal expansion of the ductal structures comprising cholangiocytes. In contrast, Pten::Keap1-Alb::$Nrf2^{+/-}$ mice survived beyond 1 month, but these mice developed severe polycystic liver fibrosis, with the increased proliferation of cholangiocytes. These phenotypes were not observed in Pten::Keap1-Alb::$Nrf2^{-/-}$ mice, indicating the Nrf2 dependency of the phenotypes. The forced activation of Nrf2 in Pten-deficient livers results in consequences with respect to liver pathology that are completely different from those of single Pten deficiency in mice. Notably, we observed that the expansion of Nrf2 function in Pten and Keap1 double-knockout mice is established by the simultaneous inactivation of two distinct Nrf2 degradation pathways. Thus, the liver-specific disruption of *Keap1* and *Pten* establishes a new Nrf2-dependent molecular network, promoting proliferation of hepatocytes and cholangiocytes and skewing cell lineage development toward cholangiocytes.

MATERIALS AND METHODS

Mice. $Pten^{flox/flox}$, $Keap1^{flox/flox}$, and $Nrf2^{-/-}$ mice were previously described (18, 20, 21). The *Albumin*-Cre transgenic mouse was purchased from The Jackson Laboratory (Bar Harbor, ME) (22). These crosses generated $Pten^{flox/flox}$ (control), $Pten^{flox/flox}$::*Albumin*-Cre (Pten-Alb), $Keap1^{flox/flox}$::*Albumin*-Cre (Keap1-Alb), $Pten^{flox/flox}$::$Keap1^{flox/flox}$:: *Albumin*-Cre (Pten::Keap1-Alb), $Pten^{flox/flox}$::$Keap1^{flox/flox}$::*Albumin*-Cre:: $Nrf2^{-/-}$ (Pten::Keap1-Alb::$Nrf2^{-/-}$), and $Pten^{flox/flox}$::$Keap1^{flox/flox}$::*Albumin*-Cre::$Nrf2^{+/-}$ (Pten::Keap1-Alb::$Nrf2^{+/-}$) mice. A Rosa-26 reporter (R26R) mouse (23) was used for the β-galactosidase assay. DNA was obtained from each mouse and genotyped using PCR. The mice were provided water and rodent chow *ad libitum*. All mice were maintained under specific-pathogen-free conditions and treated according to the regulations of The Standards for Human Care and Use of Laboratory Animals of Tohoku University and Guidelines for Proper Conduct of Animal Experiments of the Ministry of Education, Culture, Sports, Science, and Technology of Japan. The plasma was analyzed using Fuji Dri-Chem 7000 (Fujifilm Corp., Tokyo, Japan) to detect alanine transferase (ALT), aspartate transferase (AST), lactate dehydrogenase (LDH), total cholesterol (TCHO), total bilirubin (TBIL), direct bilirubin (DBIL), albumin (ALB), uric acid (UA), and blood urea nitrogen (BUN).

Immunoblot analysis. The tissues were homogenized in 9 volumes of 0.25 M sucrose, and the 10% homogenate was filtered through a 100-μm-pore-size membrane. The nuclear fraction was prepared using Dignam's method with some modifications (24). The cells were lysed in SDS sample buffer (50 mM Tris-HCl [pH 6.8], 10% glycerol, 2% SDS). The protein concentration was determined using a bicinchoninic acid (BCA) protein assay kit (Pierce Biotechnology, Rockford, IL), with bovine serum albumin as the standard. The samples were resolved using SDS-polyacrylamide gel electrophoresis and transferred onto a polyvinylidene difluoride membrane (Millipore, Billerica, MA). The following antibodies were used: anti-Nrf2 (25), anti-Keap1 (26), anti-Pten (catalog no. 9559; Cell Signaling Technology Inc., Danvers, MA), anti-LaminB (catalog no. sc-6217; Santa Cruz Biotechnology Inc., Dallas, TX), anti-Nqo1 (catalog no. ab2346; Abcam PLC, Cambridge, United Kingdom), anti-pAkt (T308) (catalog no. 9275; Cell Signaling Technology), anti-pAkt (S473) (catalog no. 9271; Cell Signaling Technology), anti-Akt (catalog no. 9272; Cell

TABLE 1 Primers and probes used in the RT-qPCR[a]

Primer	Oligonucleotide sequence	Reference
G6pc-F	5′-CGACTCGCTATCTCCAAGTGA-3′	48
G6pc-R	5′-GTTGAACCAGTCTCCGACCA-3′	
Alb-F	5′-GACGTGTGTTGCCGATGAGT-3′	
Alb-R	5′-GTTTTCACGGAGGTTTGGAATG-3′	
Krt19-F	5′-CGGTGGAAGTTTTAGTGGGA-3′	49
Krt19-R	5′-AGTAGGAGGCGAGACGATCA-3′	
Trop2-F	5′-CTGACCTAGACTCCGAGCTG-3′	50
Trop2-R	5′-CGGCCCATGAACAGTGACTC-3′	
Ggt1-F	5′-AACAGGAGCAAGAGTGGGAC-3′	51
Ggt1-R	5′-GGTGGCCTCCATTTATTGC-3′	
Gclc-F	5′-ATCTGCAAAGGCGGCAAC-3′	11
Gclc-R	5′-ACTCCTCTGCAGCTGGCTC-3′	
Gclc-P	5′-FAM-ACGGGTGCAGCAAGGCCCA-TAMRA-3′	
Gpx2-F	5′-TGTCAGAACGAGGAGATCCTG-3′	11
Gpx2-R	5′-GACTAAAGGTGGGCTGGTACC-3′	
Gpx2-P	5′-FAM-CAATACCCTCAAGTATGTCCGACCTG-TAMRA-3′	
Hes1-F	5′-TCAACACGACACCGGACAAAC-3′	11
Hes1-R	5′-ATGCCGGGAGCTATCTTTCTT-3′	
Jag1-F	5′-ATGCAGAACGTGAATGGAGAG-3′	
Jag1-R	5′-GCGGGACTGATACTCCTTGAG-3′	
rRNA-F	5′-CGGCTACCACATCCAAGGAA-3′	11
rRNA-R	5′-GCTGGAATTACCGCGGCT-3′	
rRNA-P	5′-FAM-TGCTGGCACCAGACTTGCCCTC-TAMRA-3′	

[a] FAM, 6-carboxyfluorescein; RT-qPCR, reverse transcription-quantitative PCR; TAMRA, 6-carboxytetramethylrhodamine.

Signaling Technology), anti-phosphorylated glycogen synthase kinase (pGSK)3α/β (Ser21/9; GSK3α preferred, catalog no. 9327; Cell Signaling Technology), anti-GSK3α/β (catalog no. 5676; Cell Signaling Technology), and anti-α-tubulin (catalog no. T9026; Sigma-Aldrich).

Histological analysis. The livers were fixed in Mildform 10N (Wako Pure Chemical Industries, Ltd., Osaka, Japan) and embedded in paraffin for staining with hematoxylin and eosin (HE) and Masson trichrome. For immunohistochemical staining, the livers were processed as previously described (27), using anti-cytokeratin 19 (anti-CK19) antibody (28). The positive reactivity was visualized through sequential incubation with EnVision+ Dual Link System-horseradish peroxidase (HRP) (Dako) and diaminobenzidine (DAB) staining. Hematoxylin was used for nuclear counterstaining. Using a Zamboni-fixed frozen section, immunohistochemical staining against anti-Trop2 (catalog no. AF1122; R&D Systems) and anti-EpCAM (catalog no. 118201; BioLegend) antibodies was performed according to the methods described in a previous report (29) using an LSM 510 Meta confocal microscope equipped with ZEN2008 software (Carl Zeiss, Oberkochen, Germany). X-Gal (5-bromo-4-chloro-3-indolyl-β-ᴅ-galactopyranoside) staining was performed according to the method described in a previous report (30) with slight modifications.

RNA purification and reverse transcription-quantitative PCR (RT-qPCR). Total RNA was isolated from the liver using Isogen (Nippon Gene) and transcribed into cDNA using SuperScript III reverse transcriptase (Life Technologies Corp., Carlsbad, CA). qPCR analysis was performed using the Applied Biosystems 7300 PCR system and qPCR Mas-
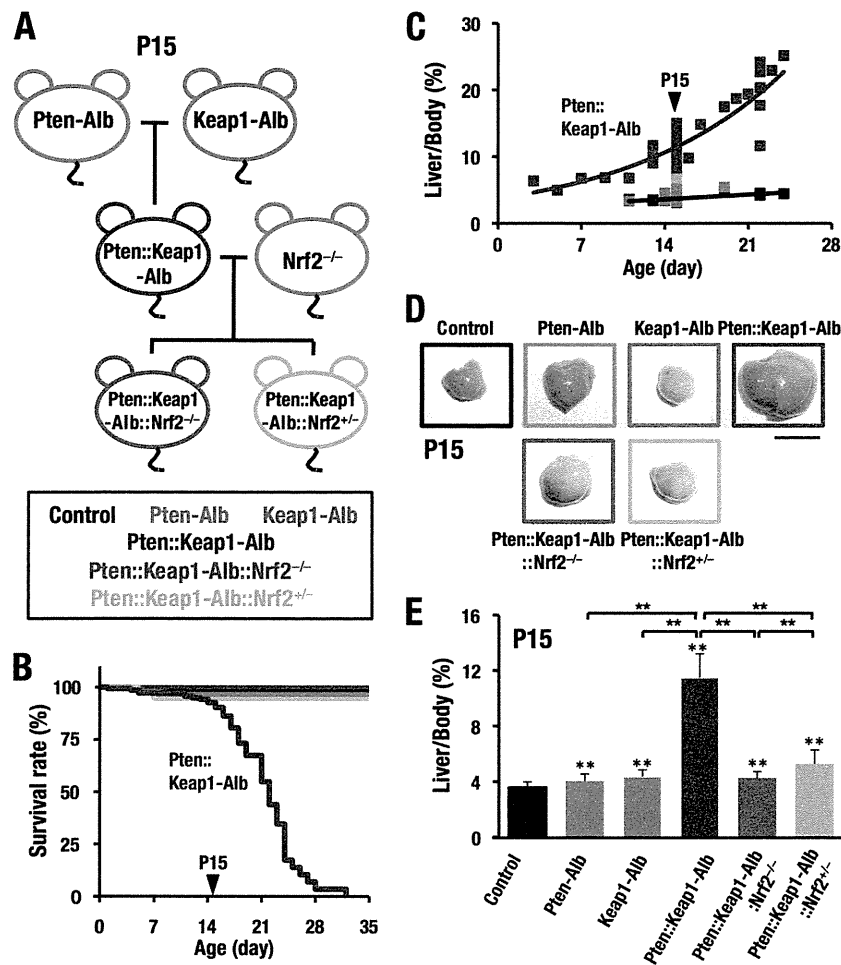
− 86 −

FIG 1 Lethality and hepatomegaly in Pten::Keap1-Alb mice. (A) Mating strategy for the generation of compound mutant mice of *Pten*, *Keap1*, and *Nrf2* genes. A detailed examination was conducted on postnatal day 15 (P15). (B) Survival rates up to P35 ($n \geq 50$). (C) Changes in liver-to-body-weight ratios to P28 ($n = 11$ to 53). (D) Representative macroscopic observation of the livers at P15. The scale bar corresponds to 1 cm. (E) Liver-to-body-weight ratios at P15 ($n = 12$ to 44). **, $P < 0.01$.

termix Plus (Eurogentec) or Power SYBR green PCR master mix (ABI). The data were normalized to rRNA expression. The primers and probes used for amplification of cDNAs are described in Table 1.

Microarray analysis. Total RNA from the liver was labeled with Cy3. The samples were hybridized to whole-mouse-genome Oligo DNA Microarray kit ver2.0 (Agilent Technologies, Inc., Santa Clara, CA) according to the manufacturer's protocol. Arrays were scanned using a G2539A microarray scanner system (Agilent), and the resulting data were analyzed using GeneSpring GX software (Agilent).

Statistical analysis. The average values were calculated, and the error bars indicate standard deviations. The differences were analyzed using Student's t test. $P < 0.05$ was considered statistically significant.

Microarray data accession number. The microarray data obtained in this study have been submitted to the Gene Expression Omnibus (GEO) database (http://www.ncbi.nlm.nih.gov/geo/) and assigned GEO accession number GSE50575.

RESULTS

Simultaneous disruption of *Pten* and *Keap1* in the liver results in hepatomegaly and lethality. We initially hypothesized that the constitutive stabilization of Nrf2 exacerbates liver carcinogenesis caused by Pten disruption. To address this hypothesis, we conducted a detailed analysis of *Pten* and *Keap1* double-mutant mice, in which both genes were deleted through Cre recombinase ex-

pression under conditions the regulation of the *Albumin* gene (Pten::Keap1-Alb mice). We compared the Pten::Keap1-Alb mice with Pten^flox/flox^ (control) mice and *Pten* single-mutant mice or *Keap1* single-mutant mice (Pten-Alb or Keap1-Alb mice, respectively). The mating strategy for the generation of *Pten* and *Keap1* compound mutant mice is shown in Fig. 1A. The results for the control, Pten-Alb, Keap1-Alb, and Pten::Keap1-Alb mice are depicted in black, red, light blue, and dark blue, respectively, in this figure and in the remaining figures shown in this study.

We observed that Pten::Keap1-Alb mice were born with Mendelian inheritance, and the appearance of the newborns was normal. The body weight gain of double-knockout mice was indistinguishable from that of control or individual single-knockout mice (data not shown). The body weights at postnatal day 15 (P15) were comparable in all genotypes examined (data not shown). Surprisingly, the Pten::Keap1-Alb mice started dying after the second week, and all the mice of this genotype died within 35 days after birth (Fig. 1B). We observed slight abdominal swelling of the double-mutant mice at 2 weeks of age (data not shown). Therefore, we examined the livers of the Pten::Keap1-Alb mice at P15. Figure 1C shows the liver-to-body-weight ratio of the Pten::Keap1-Alb mice (dark

— 87 —

blue squares) in comparison with control (black), Pten-Alb (red), and Keap1-Alb (light blue) mice. We observed that the livers of the double-knockout mice became gradually larger after birth and were markedly enlarged by P15 (Fig. 1C and D). While the magnitude of hepatomegaly was markedly significant in the Pten::Keap1-Alb double-knockout mice, the single knockouts of *Pten* or *Keap1* (Pten-Alb or Keap1-Alb mice) showed slight but significant hepatomegaly (Fig. 1E).

A closer examination of the dissected livers revealed the enlargement of the liver of the double-knockout mice, but no whitish appearance or signs of liver steatosis, characteristic phenotypes in mature Pten-Alb mice, were observed (18) (Fig. 1D). The livers of Pten single-knockout mice were also normal in appearance at P15. Notably, the livers of the Pten::Keap1-Alb mice were yellowish, indicating the development of jaundice (Fig. 1D). In addition, the plasma and urine of these mice were also yellowish (data not shown). These results demonstrate that the double deletion of *Pten* and *Keap1* in the liver results in juvenile death and abnormal hepatomegaly.

Hepatomegaly and lethality observed in *Pten* and *Keap1* double-knockout mice are Nrf2 dependent. Because one of the most prominent targets of Keap1-mediated ubiquitination is Nrf2, we hypothesized that Nrf2 plays a role in the hepatomegaly and lethality of double-mutant mice. To examine this hypothesis, we generated Pten::Keap1-Alb::Nrf2$^{-/-}$ and Pten::Keap1-Alb::Nrf2$^{+/-}$ mice by crossing Pten::Keap1-Alb mice and *Nrf2*-null mice, which do not show any apparent abnormalities in livers. The mating strategy for the generation of the compound mutant for *Pten*, *Keap1*, and *Nrf2* genes in mice is also shown in Fig. 1A. The results for the Pten::Keap1-Alb::Nrf2$^{-/-}$ and Pten::Keap1-Alb::Nrf2$^{+/-}$ mice are depicted in dark green and light green, respectively, in this figure and in the remaining figures shown in this study.

Notably, the lethality of Pten::Keap1-Alb mice was clearly abrogated in the *Nrf2*-null background (Fig. 1B). As a result of deleting *Nrf2*, the liver enlargement in the double-mutant mice was reduced to levels similar to those observed in the single-knockout mouse (Fig. 1C to E). Even the single-allele deletion of *Nrf2* was effective for the alleviation of the lethality and liver phenotypes. Thus, these results demonstrate that the Pten::Keap1-Alb mice display hepatomegaly and eventual lethality that is Nrf2 dependent.

***Pten* and *Keap1* double-mutant mice display cholangiocyte expansion and liver dysfunction.** Because Pten::Keap1-Alb mice died at approximately 2 weeks of age, we selected P15 as a time point for the pathological analyses. The histological examination of Pten::Keap1-Alb mouse livers using Masson trichrome staining revealed a marked increase of tubular structures, primarily bile ducts, and connective tissue in the region of the hepatic triad, which is the anatomically close association of hepatic artery, vein, and bile duct. Masson trichrome staining enabled clearer detection of collagen fibers and tubular structures than hematoxylin-eosin staining. The features observed in Pten::Keap1-Alb mouse livers were completely absent in control, Pten-Alb, and Keap1-Alb mice (Fig. 2Aa, b, e, and f and data not shown). We confirmed the increase of cholangiocytes using CK19 staining (28). CK19-positive staining abnormally accumulated in the double-mutant livers (Fig. 2Aj). There were no histological signs of steatosis in the livers of Pten::Keap1-Alb mice.

We also examined biochemical parameters in the blood of these double-mutant mice (Fig. 2B, left four bars). Levels of indicators of liver damage, alanine transferase (ALT), aspartate transferase (AST), and lactate dehydrogenase (LDH), were all higher in Pten::Keap1-Alb mice than in control and single-mutant mice. Total cholesterol (TCHO) levels and the direct bilirubin/total bilirubin (DBIL/TBIL) ratio were both increased in Pten::Keap1-Alb mice, suggesting the presence of bile congestion in the livers of the Pten::Keap1-Alb mice. We also examined albumin (ALB) as a marker of liver function and observed that the level of this protein was maintained within a normal range in the plasma of Pten::Keap1-Alb mice, although the plasma ALB level was slightly reduced in Keap1-Alb single-knockout mice. The biochemical examination together with the histological analysis indicates that Pten::Keap1-Alb mice display abnormal cholangiocyte expansion concomitant with cholestasis and liver damage.

Abnormal expansion of cholangiocytes and liver damage in *Pten* and *Keap1* double-mutant mice are Nrf2 dependent. To determine whether the abnormal expansion of cholangiocytes and the liver damage were provoked by the increase in Nrf2, we examined the livers of Pten::Keap1-Alb::Nrf2$^{-/-}$ triple-mutant mice. The histological examination revealed the disappearance of abnormal bile duct formation and connective tissues (Fig. 2Ac and g). The accumulation of CK19-positive cholangiocytes in double-mutant mice was abrogated in Pten::Keap1-Alb::Nrf2$^{-/-}$ mice (Fig. 2Ak). Elevated levels of ALT, AST, LDH, and TCHO and the DBIL/TBIL ratio in Pten::Keap1-Alb mice were all reduced in Pten::Keap1-Alb::Nrf2$^{-/-}$ mice to control levels (Fig. 2B, dark green bars). The ALB level in Pten::Keap1-Alb::Nrf2$^{-/-}$ mice was not different from that in mice of the other genotypes (Fig. 2B, dark green bars). We concluded that constitutively stabilized Nrf2 mediates cholangiocyte expansion and liver damage in the absence of Pten.

To further delineate the precise contribution of Nrf2, we examined the effect of the single-allele disruption of Nrf2 in the Pten::Keap1-Alb background. In the heterozygote livers, the CK19-positive cholangiocytes did not increase substantially (Fig. 2Ad, h, and l), and the biochemical parameters were within the normal range (Fig. 2B, light green bars). However, further examination of the livers of Pten::Keap1-Alb::Nrf2$^{+/-}$ mice revealed mild fibrosis spreading from the hepatic triad (Fig. 2Ad and h). Thus, we propose that chronic exposure to mild Nrf2 signals under conditions of Pten deficiency might provoke unexpected pathologies in heterozygote livers.

***Pten* and *Keap1* double-mutant cells contribute to cholangiocyte expansion.** To determine whether the cholangiocyte expansion in Pten::Keap1-Alb mouse livers were primarily derived from *Pten* and *Keap1* double-mutant cells, we performed a lineage-tracing analysis using Rosa-26 reporter mice, in which the floxed β-galactosidase reporter gene is integrated into the Rosa-26 locus. It has been reported that the majority of hepatocytes and cholangiocytes can be monitored by crossing the Rosa-26 reporter mice with *Albumin*-Cre mice (19). This double-lineage labeling by β-galactosidase in this monitoring line of mice demonstrates that the albumin promoter is functional in hepatoblasts, a common progenitor of hepatocytes and cholangiocytes (31). We observed that, in Pten::Keap1-Alb mice crossed with Rosa-26 reporter mice, not only hepatocytes but also all expanded cholangiocytes were positively stained for the β-galactosidase activity (Fig. 3B and D). The LacZ-positive tubular structures near the portal vein were CK19-positive cholangiocytes (Fig. 3F and H). Both hepatocytes
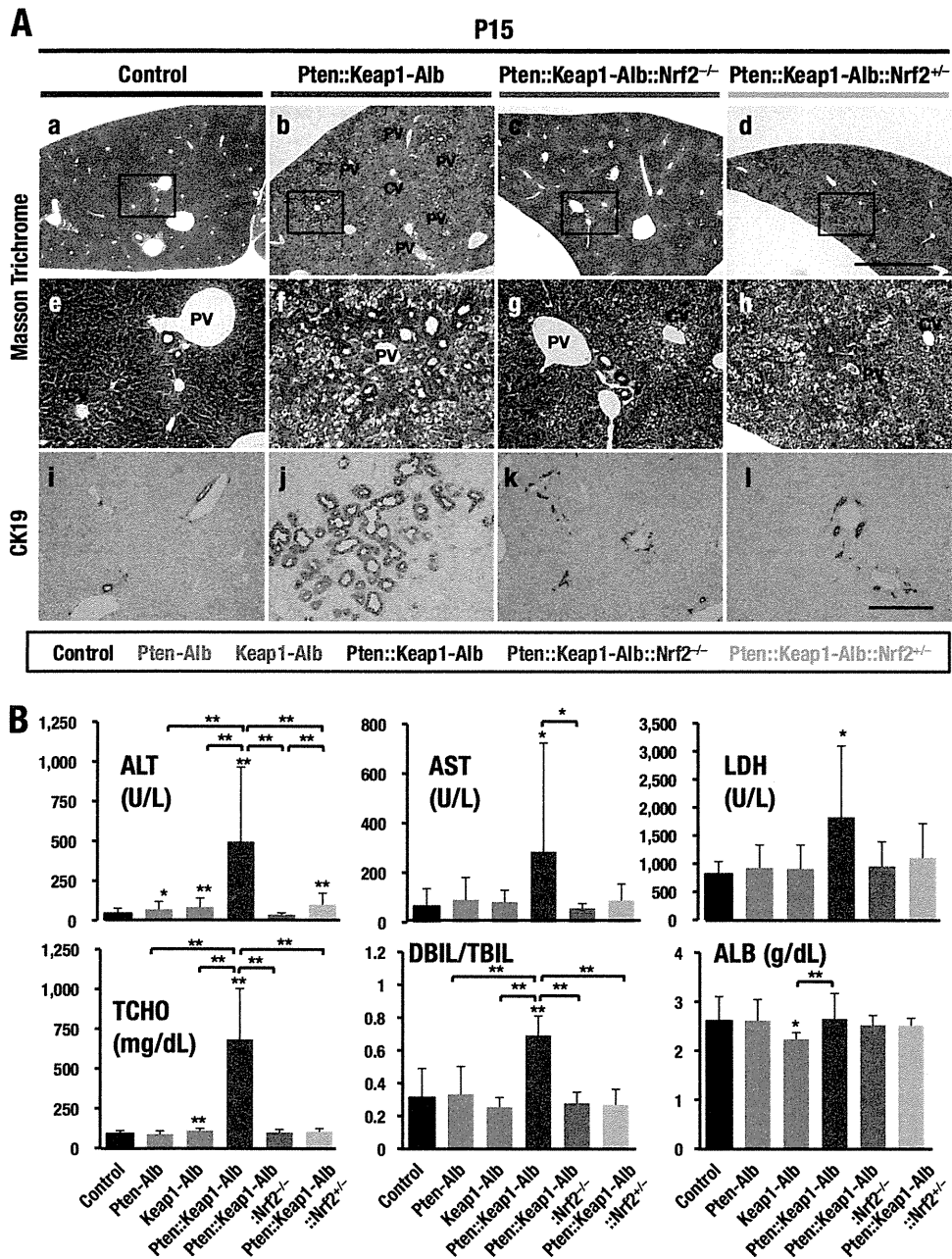
− 88 −

A

P15

FIG 2 Increase in cholangiocytes in the Pten::Keap1-Alb mouse livers. (A) Histological analysis of the livers. Results of Masson trichrome staining (a to h) and immunohistochemistry using the anti-CK19 antibody (i to l) at P15 are shown. PV, portal vein; CV, central vein. The scale bars correspond to 1 mm (a to d) and 200 μm (e to l). (B) Serum biochemical test, measuring markers for liver injury (ALT, AST, and LDH), TCHO, DBIL/TBIL ratio, and ALB at P15 (n = 8 to 27). *, $P < 0.05$; **, $P < 0.01$. Asterisks without brackets indicate the comparison with control mice.

and cholangiocytes in Pten::Keap1::R26R mice without *Albumin*-Cre (Pten::Keap1::R26R) were negative for LacZ staining (Fig. 3A and C), and the tubular structures with CK19-positive staining were not increased in these mice (Fig. 3E and G). This result indicates that Pten::Keap1 double-mutant cells contribute to cholangiocytes, suggesting that the differentiation or proliferation of cholangiocytes was promoted through the simultaneous disruption of *Pten* and *Keap1*.

Single-allele deletion of *Nrf2* delays but does not rescue the lethality of Pten::Keap1-Alb mice. Because the livers of Pten::

Keap1-Alb::Nrf2$^{+/-}$ mice showed mild fibrosis (Fig. 2Ad and h), we continued the observation of the mice together with those of other genotypes, except for Pten::Keap1-Alb mice, which died by 1 month of age (Fig. 4A; also Fig. 1B). Pten::Keap1-Alb::Nrf2$^{+/-}$ mice started dying after 2 months of age and exhibited progressive hepatomegaly until 7 months of age, by which time all the mice were dead (Fig. 4B and C). However, Pten::Keap1-Alb::Nrf2$^{-/-}$ mice survived the entire period of observation, as did the control, Pten-Alb, and Keap1-Alb mice (Fig. 4B). Pten::Keap1-Alb:: Nrf2$^{-/-}$ mice also exhibited slight hepatomegaly compared with
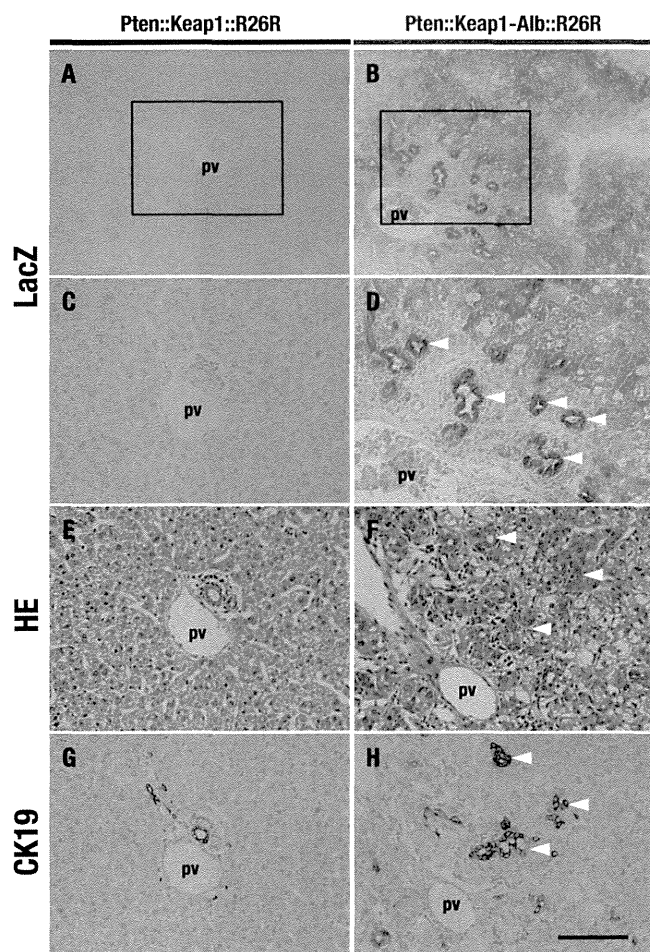
— 89 —

FIG 3 Expanded cholangiocytes are derived from *Pten* and *Keap1* doubly deficient cells. Liver sections of Pten::Keap::R26R and Pten::Keap1-Alb::R26R mice at P15 were subjected to LacZ staining (A to D), HE staining (E and F), and immunohistochemistry using the anti-CK19 antibody (G and H). Arrowheads indicate tubular structures of cholangiocytes. pv, portal vein. The scale bars correspond to 200 μm (A and B) and 100 μm (C to H).
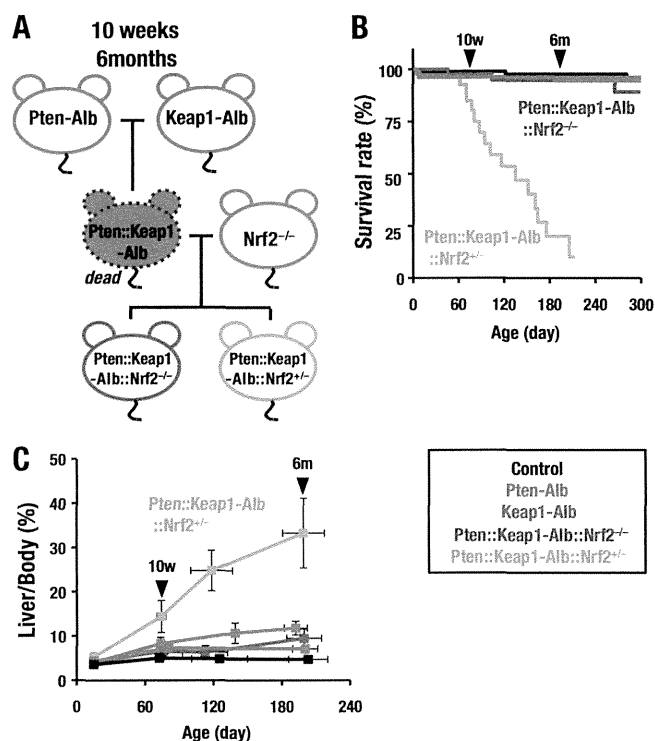

FIG 4 Pten::Keap1-Alb::Nrf2$^{+/-}$ mice demonstrate progressive hepatomegaly and die by 7 months of age. (A) Compound mutant mice of *Pten*, *Keap1*, and *Nrf2* genes analyzed at 10 weeks. Pten::Keap1-Alb mice that were lethal by 1 month were not included. (B) Survival rates at up to 240 days after birth ($n \geq 50$). (C) Changes in the liver-to-body-weight ratios up to 240 days ($n = 2$ to 43).

control mice, but the magnitude of the hepatomegaly was comparable to that of Pten-Alb and Keap1-Alb mice (Fig. 4C).

Cholangiocyte expansion is apparent in Pten::Keap1-Alb::Nrf2$^{+/-}$ liver at 10 weeks. At 10 weeks of age, female and male Pten-Alb mice exhibited a slight but significant increase in their liver-to-body-weight ratios (Fig. 5A, red bars), consistent with a previous report that Pten-Alb mice develop steatosis after 10 weeks (18). Keap1-Alb mice also displayed an increase in the ratio to a similar extent (Fig. 5A, light blue bars). In contrast, Pten::Keap1-Alb::Nrf2$^{+/-}$ mice, both female and male, showed dramatically increased liver-to-body-weight ratios at 10 weeks of age (Fig. 5A, light green bars), whereas Pten::Keap1-Alb::Nrf2$^{-/-}$ mice did not show any significant hepatomegaly (Fig. 5A, dark green bars). Surprisingly, Pten::Keap1-Alb::Nrf2$^{+/-}$ mice displayed the abnormal cholangiocyte expansion near the hepatic triad at 10 weeks (Fig. 5Be, j, and o), which was completely absent in control (Fig. 5Ba, f, and k), Pten-Alb (Fig. 5Bb, g, and l), and Keap1-Alb (Fig. 5Bc, h, and m) mice. Interestingly, mild expansion of cholangiocytes was observed in Pten::Keap1-Alb::Nrf2$^{-/-}$ mice (Fig. 5Bd, i, and n), implying the presence of an Nrf2-independent factor that promotes cholangiocyte expansion.

Pten::Keap1-Alb::Nrf2$^{+/-}$ mice develop polycystic liver fibrosis. In mice at 6 months of age, the appearance of Pten::Keap1-Alb::Nrf2$^{+/-}$ liver was dramatic. The Pten::Keap1-Alb::Nrf2$^{+/-}$ liver was significantly enlarged with a reddish brown color (Fig. 6A). Closer observation of the Pten::Keap1-Alb::Nrf2$^{+/-}$ liver revealed a multiple cystic appearance, and polycystic structures were confirmed in a section of the liver (Fig. 6B). CK19-positive tubular structures with fibrotic interstitial tissues occupied large portions of liver of Pten::Keap1-Alb::Nrf2$^{+/-}$ mice (Fig. 6Ce, j, and o), while healthy hepatocytes were hardly detected. In Pten::Keap1-Alb::Nrf2$^{+/-}$ mice, there were no signs of steatosis or carcinogenesis, which was different from our initial expectation.

In contrast, the livers of Pten-Alb mice and Pten::Keap1-Alb::Nrf2$^{-/-}$ mice did not develop any tumors but were whitish and slightly enlarged compared with control and Keap1-Alb livers (Fig. 6A). The histological analysis revealed severe steatosis in the pericentral vein area in Pten-Alb (Fig. 6Cb, g, and l) and Pten::Keap1-Alb::Nrf2$^{-/-}$ livers (Fig. 6Cd, i, and n), which was not observed in control (Fig. 6Ca, f, and k), Keap1-Alb (Fig. 6Cc, h, and m), or Pten::Keap1-Alb::Nrf2$^{+/-}$ (Fig. 6Ce, j, and o) livers. The mild expansion of cholangiocytes in Pten::Keap1-Alb::Nrf2$^{-/-}$ livers progressed at 6 months compared with 10 weeks (Fig. 6Cd, i, and n), but the severity was far less than the cholangiocyte expansion observed in Pten::Keap1-Alb::Nrf2$^{+/-}$ mice (Fig. 6Ce, j, and o), indicating that Nrf2 is the most critical factor in the progressive expansion of tubular structures lined with cholangiocytes. We surmise that an alternative substrate of Keap1 is responsible for the Nrf2-independent cholangiocyte expansion.

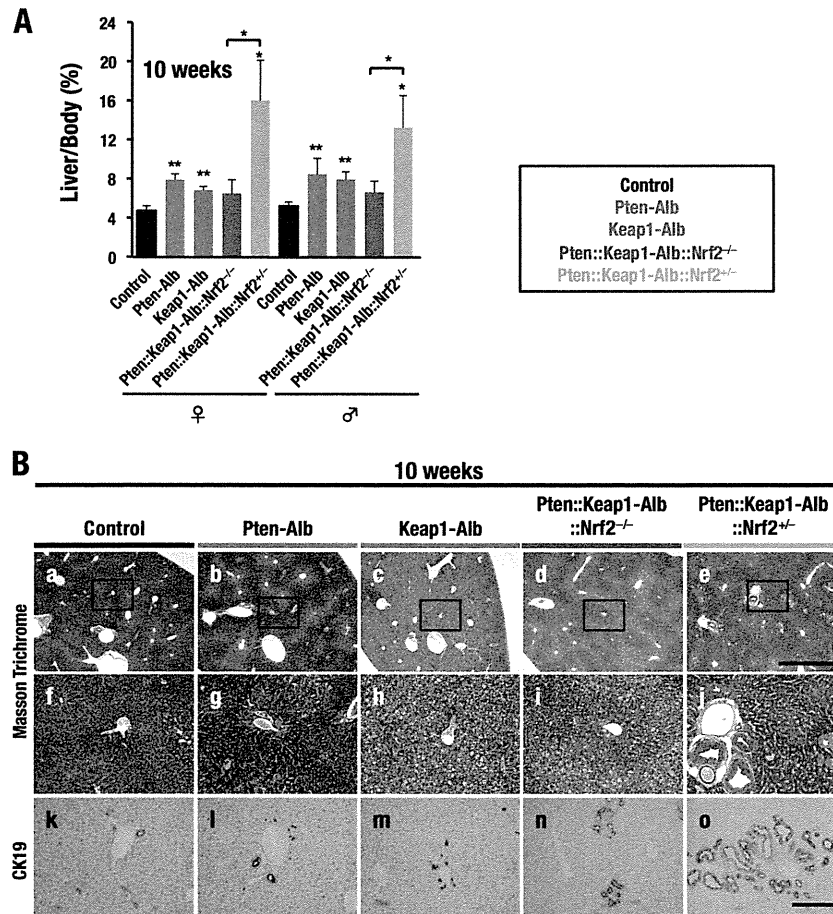**FIG 5** Cholangiocytes expansion in Pten::Keap1-Alb::Nrf2$^{+/-}$ mouse livers at 10 weeks. (A) Liver-to-body-weight ratios at 10 weeks ($n = 3$ to 10). More than 3 mice were independently examined for males and females of each genotype. *, $P < 0.05$; **, $P < 0.01$. Asterisks without brackets indicate the comparison with control mice. (B) Histological analysis of the livers at 10 weeks. Masson trichrome staining (a to j) and immunohistochemistry using the anti-CK19 antibody (k to o) are shown. The scale bars correspond to 1 mm (a to e) and 200 μm (f to o).

Gene expression profiles in Pten::Keap1-Alb mouse livers. To address the molecular mechanisms underlying cholangiocyte expansion, we performed a microarray analysis of Pten::Keap1-Alb, control, Keap1-Alb, and Pten-Alb mouse livers at P15. To delineate the Nrf2 dependency of the cholangiocyte expansion, we also conducted microarray analysis using Pten::Keap1-Alb::Nrf2$^{-/-}$ mouse livers. Consistent with the results of the pathological analyses, the majority of cholangiocyte-specific or oval cell/liver progenitor cell (LPC)-specific gene markers were dramatically upregulated in Pten::Keap1-Alb mice compared with control, Keap1-Alb, or Pten-Alb mouse livers (Fig. 7). However, hepatocyte-specific gene markers were decreased in Pten::Keap1-Alb livers.

This upregulation of cholangiocyte or LPC-specific gene markers in Pten::Keap1-Alb mouse livers was mostly cancelled in Pten::Keap1-Alb::Nrf2$^{-/-}$ mouse livers. Similarly, the expression of hepatocyte-specific genes was recovered in Pten::Keap1-Alb::Nrf2$^{-/-}$ mouse livers. These results indicate that the upregulation of cholangiocyte-specific genes and downregulation of hepatocyte-specific genes in Pten::Keap1-Alb mouse livers reflect an increase in Nrf2.

Nrf2 activation contributes to the emergence of Trop2-EpCAM double-positive cells in Pten::Keap1-Alb mouse livers.

To validate the results of the microarray analyses, we then performed real-time quantitative PCR. Consistent with the results of the microarray analyses, expression of the cholangiocyte genes, including Krt19, Ggt1, and Spp1, was also increased in Pten::Keap1-Alb mice (Fig. 8A). The increase was significantly abrogated in Pten::Keap1-Alb::Nrf2$^{-/-}$ mice. Conversely, expression of the hepatocyte genes, including Alb and G6pc, was indeed decreased in Pten::Keap1-Alb mice, and this decrease in hepatocyte gene expression was abrogated by the simultaneous disruption of Nrf2 (Fig. 8B). These results further support the conclusion that increased Nrf2 activity and the loss of Pten activity contribute to the cholangiocyte expansion and the relative decrease in the hepatocyte population in the Pten::Keap1-Alb mouse liver.

We observed that Trop2 (also referred to as Tacstd2) was highly and specifically expressed in the Pten::Keap1-Alb mouse liver (Fig. 7). Trop2 has been shown to be a marker for oval cells/LPCs (32). We confirmed a 6-fold increase in Trop2 expression specifically in the Pten::Keap1-Alb mouse liver using real-time quantitative PCR (Fig. 8C).

To examine whether oval cells emerged, we conducted immunofluorescent detection of Trop2 and EpCAM in the Pten::Keap1-Alb mouse liver. As EpCAM was expressed in both cholangiocytes and oval cells, we expected the emergence of Trop2-EpCAM double-pos-
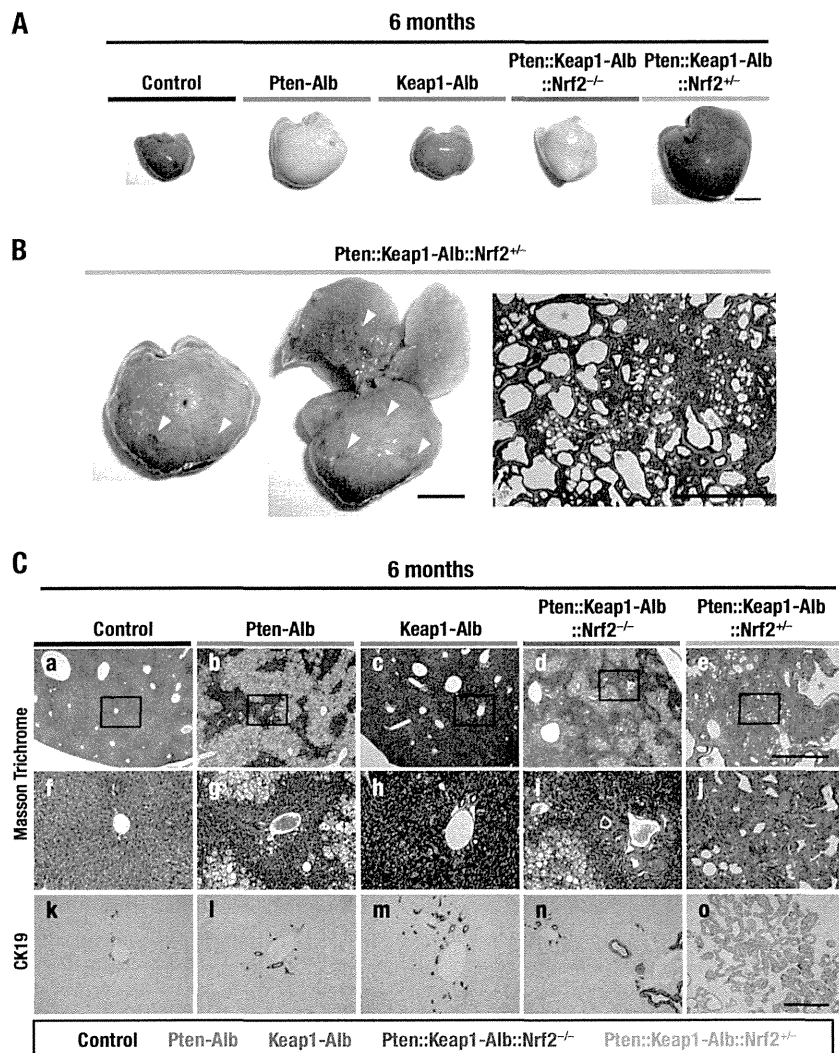
FIG 6 Development of polycystic fibrosis in Pten::Keap1-Alb::Nrf2$^{+/-}$ mice at the age of 6 months. (A) Representative macroscopic observation of the livers at 6 months of age. The scale bar corresponds to 1 cm. (B) Polycystic appearance of the Pten::Keap1-Alb::Nrf2$^{+/-}$ mouse liver in a closer view (left and middle panels) and in a section (right panel). Arrowheads indicate grossly recognizable cysts. A red asterisk indicates a cyst. The scale bars correspond to 1 cm (left and middle panels) and 1 mm (right panel). (C) Histological analysis of the livers at 6 months. Masson trichrome staining (a to j) and immunohistochemistry using the anti-CK19 antibody (k to o) are shown. The scale bars correspond to 1 mm (a to e) and 200 μm (f to o).

itive oval cells in the liver. The results revealed that a part of the cholangiocytes in Pten::Keap1-Alb mouse livers was indeed doubly positive for EpCAM and Trop2 (Fig. 8D). As oval cells have been reported to emerge in severely injured livers and contribute to the regeneration (32), these results imply that Nrf2 activation may induce oval cell expression and contribute to the abnormal expansion of cholangiocytes in Pten::Keap1-Alb mouse livers.

Enhanced phosphorylation of Gsk3 contributes to increased nuclear accumulation of Nrf2 in Pten::Keap1-Alb mice. Cholangiocyte lineage markers Ggt1 and Gstp1 have also been identified as typical Nrf2 target genes (33–36), and their expression levels were higher in Pten::Keap1-Alb mouse livers than in Keap1-Alb mouse livers (Fig. 7 and 8A). We observed that two other Nrf2 target genes, Gpx2 and Gclc, showed similar expression patterns (Fig. 9A). The increased expression levels of Gpx2 and Gclc mRNAs were completely abrogated by the concomitant deletion of Nrf2. These results are consistent with the notion that Nrf2-

dependent transcriptional activity was greatly enhanced in the Pten::Keap1-Alb liver through the increased nuclear accumulation of Nrf2 under conditions of sustained activation of the PI3K-Akt pathway (4). Indeed, when the nuclear extracts obtained from the livers of control, Pten-Alb, Keap1-Alb, and Pten::Keap1-Alb mice at P15 were examined, robust accumulation of Nrf2 protein was observed in the livers of Pten::Keap1-Alb mice compared with those of Keap1-Alb mice, accompanied by the increased expression of Nqo1 protein (Fig. 9B). The Nrf2 protein accumulation was not detectable in control and Pten-Alb mouse livers (Fig. 9B).

To understand the mechanisms underlying the increased Nrf2 accumulation in Pten::Keap1-Alb mouse livers, we examined the phosphorylation status of Gsk3 using liver protein extracts from control, Keap1-Alb, Pten-Alb, and Pten::Keap1-Alb mice. It has been shown that Gsk3, one of the main substrates of Akt, promotes Nrf2 degradation in an SCF/β-TrCP-dependent and Keap1-independent manner (37, 38). We observed that Gsk3 was

<table>
<tr><td colspan="8"></td><td>≤ -2.0 2.0 ≤
5.0 <</td></tr>
</table>

Cell type	Probe Name	Gene Symbol	Pten	Keap1	P::K	P::K::N	
Hepatocyte	A_51_P160713	Alb	-1.0	-1.1	-1.4	-1.1	albumin
	A_52_P251450	Cldn2	-1.1	1.4	-1.3	-1.2	claudin 2
	A_51_P266618	Cyp8b1	1.0	1.1	-2.5	-1.0	cytochrome P450, family 8, subfamily b, polypeptide 1
	A_51_P462385	G6pc	-1.1	1.1	-4.7	-1.0	glucose-6-phosphatase, catalytic
	A_52_P683991	Hnf4a	1.1	1.5	-1.2	1.5	hepatic nuclear factor 4, alpha
	A_52_P69656	Hnf4a	1.1	1.5	-1.1	1.2	hepatic nuclear factor 4, alpha
	A_51_P198473	Hnf4a	-1.1	1.2	-1.6	-1.5	hepatic nuclear factor 4, alpha
	A_51_P362638	Trf	1.1	1.0	-1.6	1.1	transferrin
Cholangiocyte	A_51_P155445	Abcb1a	1.2	-1.5	2.1	1.1	ATP-binding cassette, sub-family B (MDR/TAP), member 1A
	A_52_P92772	Abcb1b	1.2	-1.0	1.4	1.7	ATP-binding cassette, sub-family B (MDR/TAP), member 1B
	A_52_P170509	Abcb1b	-1.3	1.4	1.5	1.0	ATP-binding cassette, sub-family B (MDR/TAP), member 1B
	A_51_P245368	Abcb1b	-1.2	-1.2	2.1	-1.5	ATP-binding cassette, sub-family B (MDR/TAP), member 1B
	A_51_P500676	Dmbt1	2.3	43.4	18.5	2.1	deleted in malignant brain tumors 1
	A_52_P447944	Epcam	1.3	-1.3	8.1	-2.6	epithelial cell adhesion molecule
	A_51_P468073	Ggt1	1.3	31.6	258.8	1.2	gamma-glutamyltransferase 1
	A_51_P440238	Ggt6	-1.1	4.1	5.8	2.2	gamma-glutamyltransferase 6
	A_51_P374457	Gstp1	-1.2	3.3	2.4	-1.4	glutathione S-transferase, pi 1
	A_51_P374464	Gstp1	-1.1	4.2	5.8	-1.3	glutathione S-transferase, pi 1
	A_51_P484311	Hnf1b	-1.1	-1.3	-1.1	-1.5	HNF1 homeobox B
	A_52_P177699	Hnf1b	-1.0	1.0	1.3	-1.1	HNF1 homeobox B
	A_51_P312348	Krt7	1.1	1.6	17.1	1.2	keratin 7
	A_52_P410685	Krt7	1.2	1.3	14.4	1.1	keratin 7
	A_51_P356642	Krt19	1.2	2.2	13.5	1.1	keratin 19
	A_52_P214630	Sox9	1.1	1.2	7.4	-1.2	SRY-box containing gene 9
	A_51_P451606	Sox9	1.2	-1.0	4.5	-1.7	SRY-box containing gene 9
	A_52_P577484	Sox9	1.1	1.1	6.5	-1.9	SRY-box containing gene 9
	A_51_P358765	Spp1	1.7	1.1	14.2	-1.3	secreted phosphoprotein 1
	A_52_P190973	Vcl	1.0	1.3	2.3	-1.2	vinculin
	A_51_P297131	Vcl	-1.0	-1.0	1.9	-1.3	vinculin
Oval cell/Liver progenitor cell	A_52_P244193	Cd24a	1.2	1.2	6.9	1.4	CD24a antigen
	A_51_P257938	Tacstd2	3.5	-1.4	8.2	1.3	tumor-associated calcium signal transducer 2

Pten-Alb   Keap1-Alb   Pten::Keap1-Alb   Pten::Keap1-Alb::Nrf2$^{-/-}$

FIG 7 Expression of cell-specific marker genes in the liver at P15. Cell-specific gene markers were categorized into hepatocyte, cholangiocyte, and oval cell/liver progenitor cells in Pten-Alb, Keap1-Alb, Pten::Keap1-Alb, and Pten::Keap1-Alb::Nrf2$^{-/-}$ mouse livers at P15. The fold change values indicate the base 2 logarithm of the expression ratio to control mouse values.

markedly phosphorylated in Pten::Keap1-Alb mouse livers compared with control, Keap1-Alb, and Pten-Alb mouse livers (Fig. 9B). Because phosphorylated Gsk3 is inactive, these results suggest that Gsk3 phosphorylation under conditions of sustained activation of the PI3K-Akt pathway induces the increased accumulation of Nrf2. Thus, the massive accumulation of Nrf2 in Pten::Keap1-Alb livers is attributable to the simultaneous inactivation of the Keap1-dependent degradation and β-TrCP-dependent degradation of Nrf2.

Notably, Pten expression in Pten-Alb and Pten::Keap1-Alb mice was decreased but still detectable at P15, whereas Keap1 expression in Keap1-Alb and Pten::Keap1-Alb mice was almost undetectable (Fig. 9B). Therefore, to assess effects of complete Pten ablation on Nrf2 accumulation, we examined control and Pten-Alb mouse livers at the 10 weeks of age, when Pten was almost undetectable (Fig. 9B). At 10 weeks, Pten-Alb mouse livers exhibited the increased phosphorylation of Akt and Gsk3 but did not exhibit any Nrf2 accumulation above the control level. These results indicate that the β-TrCP-dependent degradation of Nrf2 is relatively minor for Nrf2 degradation compared with the Keap1 pathway. The contribution of the β-TrCP-dependent pathway to Nrf2 accumulation was detectible only when the Keap1 pathway was abrogated in the Pten::Keap1-Alb liver.

Moreover, we also examined the phosphorylation status of Akt and Gsk3 in the liver extracts from Pten::Keap1-Alb::Nrf2$^{-/-}$ mice compared with the phosphorylation status in those from Pten::Keap1-Alb mice. We observed a robust augmentation in Gsk3 phosphorylation in Pten::Keap1-Alb mouse livers, and this phosphorylation status was completely restored in Pten::Keap1-Alb::Nrf2$^{-/-}$ mouse livers (Fig. 9B). We also observed that the phosphorylation of Akt was significantly stimulated in the Pten::Keap1-Alb livers, and weak phosphorylation was observed in the absence of Nrf2 (Fig. 9B). These results are consistent with our previous observation that Nrf2 enhances the activity of the PI3K-Akt pathway (4), whose detailed mechanism remains to be elucidated.

DISCUSSION

This study revealed unique synthetic liver phenotypes driven by functional interactions between the Keap1-Nrf2 and Pten-PI3K-Akt pathways. The liver-specific double disruption of the *Pten* and *Keap1* genes results in dramatic hepatomegaly with expanded tubular structures comprising cholangiocytes and eventual periweaning lethality. Importantly, these abnormalities were all restored through the simultaneous disruption of *Nrf2*, indicating that the constitutive stabilization of Nrf2 in the liver under con-
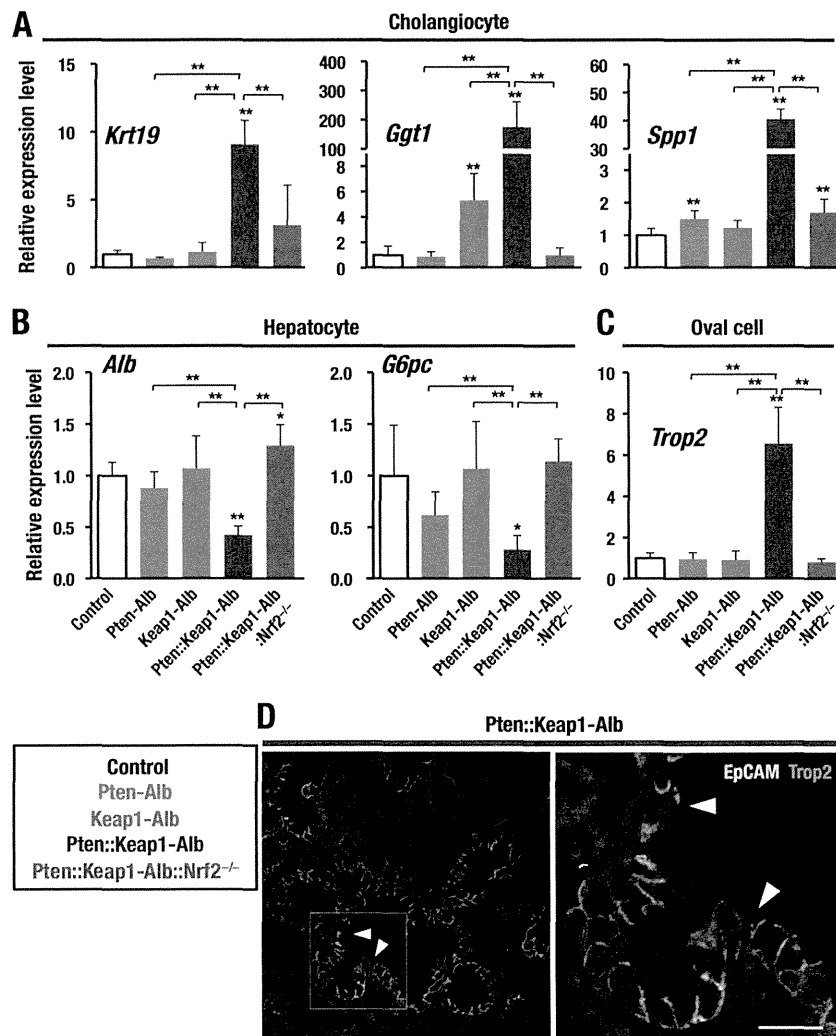
− 93 −

FIG 8 Gene expression profiles of Pten::Keap1-Alb liver. Relative expression of mRNAs in control, Pten-Alb, Keap1-Alb, Pten::Keap1-Alb, and Pten::Keap1-Alb::Nrf2$^{-/-}$ mouse livers of male mice at P15 ($n = 3$ to 6). The average values of control mice are set to 1. *, $P < 0.05$; **, $P < 0.01$. Asterisks without brackets indicate the comparison with control mice. The full gene names are listed in Fig. 7. (A) Expression levels of cholangiocyte-specific genes. (B) Expression levels of hepatocyte-specific genes. (C) Expression levels of oval cell-specific genes. (D) A representative immunofluorescent image of Pten::Keap1-Alb mouse livers using anti-EpCAM and anti-Trop2 antibodies. Higher magnification of the area surrounded by a white square is shown on the right. Arrowheads indicate the EpCAM-Trop2 double-positive cells. The scale bar corresponds to 50 μm (left panel) and 17 μm (right panel).

ditions of sustained activation of the PI3K-Akt pathway modulates cell growth and differentiation. Considering the well-characterized contribution of Nrf2 in response to stress, skewing cell lineage development is a particularly novel function of Nrf2 revealed in this study. We recently found another occasion where Nrf2 exerts the similar function, altering the lineage commitment of hematopoietic cells (52). Considering the wide-ranging expression of Nrf2, still other cell differentiation events may be under the control of Nrf2.

A characteristic histopathological feature of Pten::Keap1-Alb mice is the excessive expansion of cholangiocytes, which resembles the human pathology observed in liver cirrhosis, alcoholic liver injury, and acute hepatitis. Although the precise molecular mechanisms underlying the Nrf2-dependent expansion of cholangiocytes in Pten::Keap1-Alb mice are currently unknown, we speculate that Nrf2 promotes the differentiation of cholangiocytes at the stage of hepatoblasts on the basis of the observation

that *Pten* and *Keap1* gene disruption is initiated in hepatoblasts. It is also plausible that Nrf2 enhances the induction and differentiation of oval cells into cholangiocytes on the basis of the observation that Trop2-EpCAM double-positive cells, which are possible oval cells, are specifically induced in the livers of Pten::Keap1-Alb mice. Notably, similar phenotypes have been observed in the livers of *Fbxw7* conditional-knockout mice (39). The increased Notch pathway activity due to Fbxw7 deficiency skewed the differentiation of hepatoblasts toward the cholangiocyte lineage. In the present study, however, Notch pathway-related genes were generally not upregulated in the livers of Pten::Keap1-Alb mice, except for *Jag1* and *Hes1* (data not shown), suggesting that alternative mechanisms might operate in Pten::Keap1-Alb livers.

Another interesting histopathological alteration observed in Pten::Keap1-Alb mice is that involving liver fibrosis, especially in regions surrounding the increased cholangiocytes. It has been reported that Nrf2 activation suppresses hepatic fibrosis. For exam-
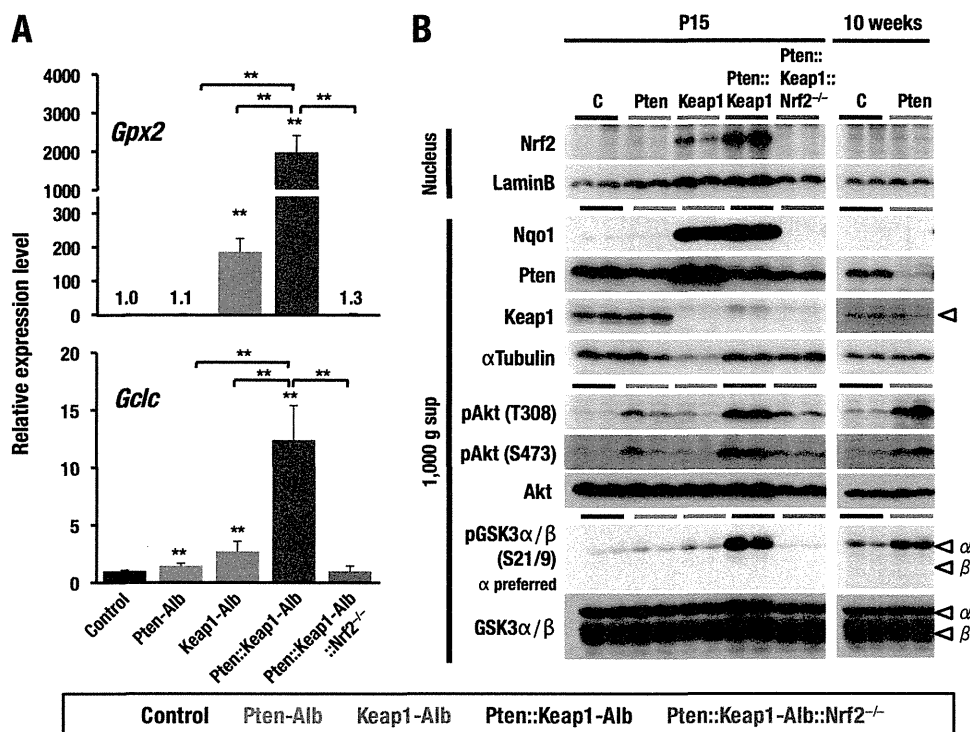
— 94 —

FIG 9 Enhancement of Nrf2 activity and the PI3K-Akt pathway in Pten::Keap1-Alb mouse livers. (A) Gene expression levels of representative Nrf2 target genes, *Gpx2* and *Gclc*, in control, Pten-Alb, Keap1-Alb, Pten::Keap1-Alb, and Pten::Keap1-Alb::Nrf2$^{-/-}$ mouse livers at P15 (n = 3 to 6). The average values of control mice are set to 1. *, $P < 0.05$; **, $P < 0.01$. Asterisks without brackets indicate the comparison with control mice. (B) Immunoblot analysis of liver extracts from control, Pten-Alb, Keap1-Alb, Pten::Keap1-Alb, and Pten::Keap1-Alb::Nrf2$^{-/-}$ mouse livers measuring the nuclear accumulation of Nrf2, reduction efficiency of Pten and Keap1, and phosphorylation of Akt and Gsk3. Nqo1 is the product of an Nrf2 target gene. Arrowheads indicate Keap1 and two isoforms of Gsk3. Control, Pten-Alb, Keap1-Alb, Pten::Keap1-Alb, and Pten::Keap1-Alb::Nrf2$^{-/-}$ mouse livers were analyzed at P15, and control and Pten-Alb mouse livers were also analyzed at 10 weeks.

ple, *Nrf2*-null mice fed a methionine- and choline-deficient diet exhibit steatohepatitis that is severer than that seen in wild-type mice (40). In such a case, fibrosis is preceded by steatosis and is considered secondary to liver damage. In contrast, our results indicate that Nrf2 activation seems to primarily promote fibrosis in the absence of Pten, because the fibrosis becomes evident prior to the cholangiocyte expansion in Pten::Keap1-Alb::Nrf2$^{+/-}$ mice. Importantly, steatosis is not detectable in either Pten::Keap1-Alb or Pten::Keap1-Alb::Nrf2$^{+/-}$ mice. Thus, the liver fibrosis observed in this study seems to be unique, as the pathology is not associated with steatosis.

In the present study, we clarified the relationship of two degradation systems which regulate Nrf2 abundance. The Keap1- and β-TrCP-dependent Nrf2 degradation pathways and their loss-of-function mutations are schematically shown in Fig. 10 (left and middle panels, respectively). Keap1 is an adaptor for Cul3-based ubiquitin ligase that is primarily located in the cytoplasm (26). The pathway involving Keap1-dependent ubiquitination and subsequent degradation of Nrf2 is the major regulatory pathway leading to the stabilization of Nrf2. In addition, the Keap1-independent degradation pathway, mediated through Cul1-based ubiquitin ligase, containing β-TrCP as an adaptor, has been reported (37, 38). Because this pathway requires the phosphorylation of Nrf2 by Gsk3, the β-TrCP-dependent degradation of Nrf2 is inhibited in the presence of the Pten deficiency, where Akt phosphorylates and inactivates Gsk3. Importantly, Nrf2 was not accumulated in Pten-Alb mice (Fig. 10, middle panel). In contrast, in

the presence of the double deficiency of the *Pten* and *Keap1* genes, where both degradation systems were inactivated, Nrf2 accumulation was dramatically increased (Fig. 10, right panel), indicating that the apparent contribution of β-TrCP-dependent degradation was observed only when the Keap1-dependent pathway was inactivated. Based on these observations, we propose that the β-TrCP-dependent mechanism contributes to the second-line degradation mechanism of Nrf2, which targets Nrf2 that has escaped from Keap1-dependent degradation. Because the β-TrCP-dependent mechanism has been implicated as a nuclear event (38), the Nrf2 that has escaped from the Keap1-dependent degradation in the cytoplasm is translocated into the nucleus and subjected to the β-TrCP-dependent degradation.

This study has substantiated two distinct Nrf2 degradation mechanisms operating *in vivo* and provided insights into the relationship between these two pathways. Based on accumulating lines of evidence, we have observed that cells adopt multilayered strategies for the Nrf2 activation/regulation. For instance, we discovered the electrophilic modification of Keap1 as a mechanism of Nrf2 stabilization/activation for the maintenance of redox homeostasis (3). We also observed that in human cancer cells, somatic mutations of the *KEAP1* or *NRF2* gene abrogate the KEAP1-mediated degradation of NRF2 (41, 42). The autophagy and mTOR pathways also critically contribute to Nrf2 activation (43, 44). In addition to Keap1-dependent regulation at the protein level, the transcriptional regulation of Nrf2 substantially influences Nrf2 activity (45, 46). Indeed, single nucleotide polymor-
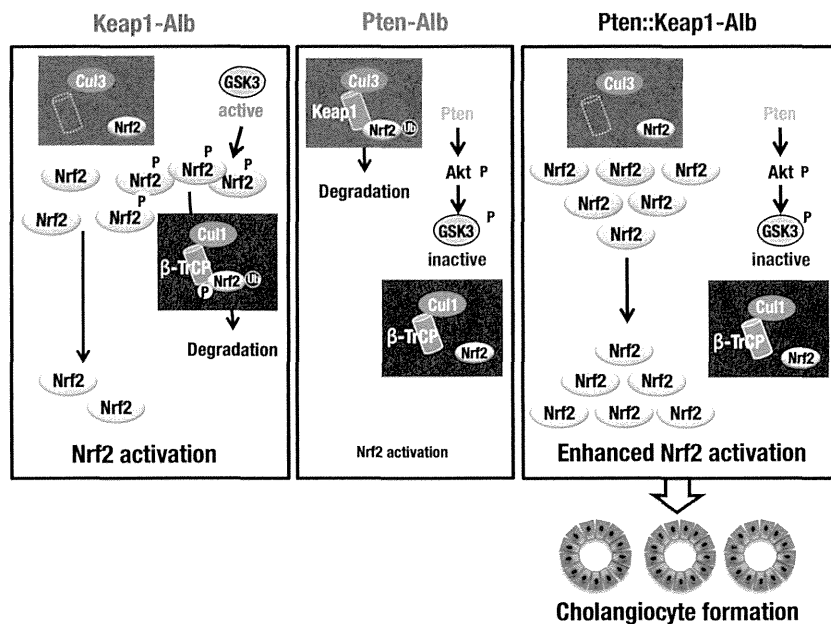
— 95 —

FIG 10 Two distinct pathways for Nrf2 degradation. Nrf2 is primarily degraded in a Keap1-Cul3-dependent manner. In Keap1-Alb mouse livers, Nrf2 escapes from the primary degradation but is subjected to secondary degradation mediated through β-TrCP-Cul1-dependent degradation, which limits Nrf2 accumulation. For secondary degradation, Nrf2 needs to be phosphorylated through Gsk3 (left panel). In Pten-Alb mouse livers, Gsk3 is inactivated but does not affect the Nrf2 abundance because the Keap1-Cul3-dependent pathway constantly degrades Nrf2 (middle panel). In Pten::Keap1-Alb mouse livers, Nrf2 escapes from primary and secondary degradation due to Keap1 deletion and Gsk3 inactivation, resulting in a robust increase of Nrf2 accumulation (right panel).

phisms in human *NRF2* and mouse *Nrf2* upstream-promoter regions alter the transcription levels of these genes, changing the overall activity of Nrf2 and its susceptibility to oxidative and xenobiotic insults. Of these layers of regulations, the β-TrCP-dependent degradation pathway is controlled through the PI3K-Akt signaling that has a profound influence on cell growth and differentiation. The PI3K-Akt pathway appears to regulate cell differentiation through Nrf2 activation under conditions that include the mitigation of Keap1-dependent degradation. Therefore, we propose that the coordinated sequential action of the Keap1- and β-TrCP-dependent degradation mechanisms forms a regulatory basis for the contribution of Nrf2 to cell lineage development.

The periweaning lethality of Pten::Keap1-Alb mice was one of the unexpected phenotypes obtained in the present study. The Pten::Keap1-Alb mice died before weaning, which was much earlier than the deaths of *Pten* or *Keap1* single-knockout mice. While we cannot identify any definitive causes of the periweaning death of the Pten::Keap1-Alb mice, we propose that the following observations might be pertinent. First, the gain in body weight of the Pten::Keap1-Alb mice was comparable to that of control mice, and the physical appearance of the mice was normal, except for mild abdominal swelling. Most of the Pten::Keap1-Alb mice died suddenly, without any apparent preceding signs. Second, we observed that the plasma levels of markers of liver injury in Pten::Keap1-Alb mice were higher than those in control mice but were not as high as those during fatal liver failure. The preliminary blood biochemistry analyses revealed that the UA level in plasma at P15 was three times higher in Pten::Keap1-Alb mice than in control mice but that the BUN score was elevated only mildly (data not shown). The elevated UA level in Pten::Keap1-Alb mice was decreased to the control level in Pten::Keap1-Alb::Nrf2$^{-/-}$ and Pten::Keap1-Alb::Nrf2$^{+/-}$ mice, showing a similar Nrf2 de-

pendency of the liver pathology and lethality. These wide-ranging observations suggest that the periweaning death of the Pten:: Keap1-Alb mice might reflect a certain organ failure(s) provoked through liver-derived general metabolic changes rather than drastic developmental defects or severe liver injury.

Pten-Alb mice serve as unique models of nonalcoholic fatty liver disease, showing the stepwise progression from steatosis, steatohepatitis, and fibrosis to tumor formation (18). We were interested in the effect of Nrf2 activation on each stage of liver pathology in the *Pten*-null background, particularly on the transition from steatosis to steatohepatitis, as oxidative stress is one of the critical factors for the transition in Pten-Alb mouse livers (18). Indeed, previous reports described how Nrf2 contributes to protection of the liver in diet-associated steatosis models (40, 47). We predicted that Nrf2 activation through Keap1 disruption would reduce reactive oxygen species and prevent the development of steatohepatitis, even in the absence of Pten. Surprisingly, however, Nrf2 activation in the *Pten*-null background (Pten::Keap1-Alb:: Nrf2$^{+/-}$ mice) completely suppressed the development of not only steatohepatitis but also steatosis or lipid accumulation in hepatocytes at 6 months of age. In contrast, Nrf2-deficient (Pten:: Keap1-Alb::Nrf2$^{-/-}$) mouse livers exhibited steatosis similar to that observed in Pten-Alb mouse livers. Thus, these results demonstrate that the Nrf2 pathway antagonizes the increased synthesis and/or storage of triglycerides in hepatocytes caused by the Pten deficiency.

Another important phenotype of Pten deficiency is cancer developing from steatohepatitis in mice that are more than 12 months of age (18, 19). This long latency period suggests that genetic alterations need to accumulate to promote carcinogenesis. Because Nrf2 enhances the establishment of malignant cancers (13, 14), we initially anticipated that we would find that Nrf2

— 96 —

activation accelerates the oncogenic process through the Pten deficiency. In contrast to our expectation, however, Pten::Keap1-Alb::Nrf2$^{+/-}$ mice did not develop cancers but displayed noncancerous hepatomegaly with cholangiocyte expansion and eventual cystic liver fibrosis. Considering the cytoprotective function of Nrf2, we propose that Nrf2 stabilization might protect cells from the progressive accumulation of genetic mutations, resulting in the inhibition of the malignant transformation of cells. In contrast, the double deletion of *Pten* and *Smad4* in the liver develops cholangiocellular carcinoma after 4 months of age, which is much faster than that in Pten-Alb mice (19), indicating that the abrogation of transforming growth factor β (TGF-β) signaling promotes carcinogenesis. Thus, the functional contributions of the Nrf2 signaling to liver carcinogenesis are fundamentally distinct from those of TGF-β signaling.

In summary, the results of the present study showed that genetic Keap1 ablation/Nrf2 activation in Pten-deficient livers generates consequences in liver pathology that are completely different from those observed in singly Pten-deficient mice. The liver-specific Pten-Keap1 double disruption results in the dramatic hepatomegaly, with expanded tubular structures comprising cholangiocytes and eventual periweaning lethality. Notably, we identified, for the first time, that the massive expansion of Nrf2 in Pten-Keap1 double-knockout mice is induced through the simultaneous inactivation of two distinct Nrf2 degradation pathways. Thus, these results have established a new Nrf2-dependent molecular network that promotes cell proliferation and skews cell lineage development.

ACKNOWLEDGMENTS

REFERENCES

1. Motohashi H, Yamamoto M. 2004. Nrf2-Keap1 defines a physiologically important stress response mechanism. Trends Mol. Med. 10:549–557. http://dx.doi.org/10.1016/j.molmed.2004.09.003.
2. Hirotsu Y, Katsuoka F, Funayama R, Nagashima T, Nishida Y, Nakayama K, Engel JD, Yamamoto M. 2012. Nrf2-MafG heterodimers contribute globally to antioxidant and metabolic networks. Nucleic Acids Res. 40:10228–10239. http://dx.doi.org/10.1093/nar/gks827.
3. Kobayashi A, Kang MI, Watai Y, Tong KI, Shibata T, Uchida K, Yamamoto M. 2006. Oxidative and electrophilic stresses activate Nrf2 through inhibition of ubiquitination activity of Keap1. Mol. Cell. Biol. 26:221–229. http://dx.doi.org/10.1128/MCB.26.1.221-229.2006.
4. Mitsuishi Y, Taguchi K, Kawatani Y, Shibata T, Nukiwa T, Aburatani H, Yamamoto M, Motohashi H. 2012. Nrf2 redirects glucose and glutamine into anabolic pathways in metabolic reprogramming. Cancer Cell 22:66–79. http://dx.doi.org/10.1016/j.ccr.2012.05.016.
5. Singh A, Happel C, Manna SK, Acquaah-Mensah G, Carrerero J, Kumar S, Nasipuri P, Krausz KW, Wakabayashi N, Dewi R, Boros LG, Gonzalez FJ, Gabrielson E, Wong KK, Girnun G, Biswal S. 2013. Transcription factor NRF2 regulates miR-1 and miR-206 to drive tumorigenesis. J. Clin. Invest. 123:2921–2934. http://dx.doi.org/10.1172/JCI66353.
6. Taguchi K, Motohashi H, Yamamoto M. 2011. Molecular mechanisms of the Keap1-Nrf2 pathway in stress response and cancer evolution. Genes Cells 16:123–140. http://dx.doi.org/10.1111/j.1365-2443.2010.01473.x.
7. Inoue D, Suzuki T, Mitsuishi Y, Miki Y, Suzuki S, Sugawara S, Watanabe M, Sakurada A, Endo C, Uruno A, Sasano H, Nakagawa T, Satoh K, Tanaka N, Kubo H, Motohashi H, Yamamoto M. 2012. Accumulation of p62/SQSTM1 is associated with poor prognosis in patients with lung adenocarcinoma. Cancer Sci. 103:760–766. http://dx.doi.org/10.1111/j.1349-7006.2012.02216.x.
8. Mitsuishi Y, Motohashi H, Yamamoto M. 2012. The Keap1-Nrf2 system in cancers: stress response and anabolic metabolism. Front. Oncol. 2:200. http://dx.doi.org/10.3389/fonc.2012.00200.
9. Wakabayashi N, Itoh K, Wakabayashi J, Motohashi H, Noda S, Takahashi S, Imakado S, Kotsuji T, Otsuka F, Roop DR, Harada T, Engel JD, Yamamoto M. 2003. Keap1-null mutation leads to postnatal lethality due to constitutive Nrf2 activation. Nat. Genet. 35:238–245. http://dx.doi.org/10.1038/ng1248.
10. Motohashi H, Katsuoka F, Engel JD, Yamamoto M. 2004. Small Maf proteins serve as transcriptional cofactors for keratinocyte differentiation in the Keap1-Nrf2 regulatory pathway. Proc. Natl. Acad. Sci. U. S. A. 101:6379–6384. http://dx.doi.org/10.1073/pnas.0305902101.
11. Taguchi K, Maher JM, Suzuki T, Kawatani Y, Motohashi H, Yamamoto M. 2010. Genetic analysis of cytoprotective functions supported by graded expression of Keap1. Mol. Cell. Biol. 30:3016–3026. http://dx.doi.org/10.1128/MCB.01591-09.
12. Motohashi H, Fujita R, Takayama M, Inoue A, Katsuoka F, Bresnick EH, Yamamoto M. 2011. Molecular determinants for small Maf protein control of platelet production. Mol. Cell. Biol. 31:151–162. http://dx.doi.org/10.1128/MCB.00798-10.
13. Satoh H, Moriguchi T, Takai J, Ebina M, Yamamoto M. 2013. Nrf2 prevents initiation but accelerates progression through the Kras signaling pathway during lung carcinogenesis. Cancer Res. 73:4158–4168. http://dx.doi.org/10.1158/0008-5472.CAN-12-4499.
14. DeNicola GM, Karreth FA, Humpton TJ, Gopinathan A, Wei C, Frese K, Mangal D, Yu KH, Yeo CJ, Calhoun ES, Scrimieri F, Winter JM, Hruban RH, Iacobuzio-Donahue C, Kern SE, Blair IA, Tuveson DA. 2011. Oncogene-induced Nrf2 transcription promotes ROS detoxification and tumorigenesis. Nature 475:106–109. http://dx.doi.org/10.1038/nature10189.
15. Stambolic V, Suzuki A, de la Pompa JL, Brothers GM, Mirtsos C, Sasaki T, Ruland J, Penninger JM, Siderovski DP, Mak TW. 1998. Negative regulation of PKB/Akt-dependent cell survival by the tumor suppressor PTEN. Cell 95:29–39. http://dx.doi.org/10.1016/S0092-8674(00)81780-8.
16. Zhang S, Yu D. 2010. PI(3)king apart PTEN's role in cancer. Clin. Cancer Res. 16:4325–4330. http://dx.doi.org/10.1158/1078-0432.CCR-09-2990.
17. Hu TH, Huang CC, Lin PR, Chang HW, Ger LP, Lin YW, Changchien CS, Lee CM, Tai MH. 2003. Expression and prognostic role of tumor suppressor gene PTEN/MMAC1/TEP1 in hepatocellular carcinoma. Cancer 97:1929–1940. http://dx.doi.org/10.1002/cncr.11266.
18. Horie Y, Suzuki A, Kataoka E, Sasaki T, Hamada K, Sasaki J, Mizuno K, Hasegawa G, Kishimoto H, Iizuka M, Naito M, Enomoto K, Watanabe S, Mak TW, Nakano T. 2004. Hepatocyte-specific Pten deficiency results in steatohepatitis and hepatocellular carcinomas. J. Clin. Invest. 113:1774–1783. http://dx.doi.org/10.1172/JCI20513.
19. Xu X, Kobayashi S, Qiao W, Li C, Xiao C, Radaeva S, Stiles B, Wang RH, Ohara N, Yoshino T, LeRoith D, Torbenson MS, Gores GJ, Wu H, Gao B, Deng CX. 2006. Induction of intrahepatic cholangiocellular carcinoma by liver-specific disruption of Smad4 and Pten in mice. J. Clin. Invest. 116:1843–1852. http://dx.doi.org/10.1172/JCI27282.
20. Itoh K, Chiba T, Takahashi S, Ishii T, Igarashi K, Katoh Y, Oyake T, Hayashi N, Satoh K, Hatayama I, Yamamoto M, Nabeshima Y. 1997. An Nrf2/small Maf heterodimer mediates the induction of phase II detoxifying enzyme genes through antioxidant response elements. Biochem. Biophys. Res. Commun. 236:313–322. http://dx.doi.org/10.1006/bbrc.1997.6943.
21. Okawa H, Motohashi H, Kobayashi A, Aburatani H, Kensler TW, Yamamoto M. 2006. Hepatocyte-specific deletion of the keap1 gene activates Nrf2 and confers potent resistance against acute drug toxicity. Biochem. Biophys. Res. Commun. 339:79–88. http://dx.doi.org/10.1016/j.bbrc.2005.10.185.
22. Postic C, Magnuson MA. 2000. DNA excision in liver by an albumin-Cre transgene occurs progressively with age. Genesis 26:149–150. http://dx.doi.org/10.1002/(SICI)1526-968X(200002)26:2<149::AID-GENE16>3.0.CO;2-V.

— 97 —

23. Soriano P. 1999. Generalized lacZ expression with the ROSA26 Cre reporter strain. Nat. Genet. 21:70–71. http://dx.doi.org/10.1038/5007.

24. Mura C, Le Gac G, Jacolot S, Ferec C. 2004. Transcriptional regulation of the human HFE gene indicates high liver expression and erythropoiesis coregulation. FASEB J. 18:1922–1924. http://dx.doi.org/10.1096/fj.04 -2520fje.

25. Maruyama A, Tsukamoto S, Nishikawa K, Yoshida A, Harada N, Motojima K, Ishii T, Nakane A, Yamamoto M, Itoh K. 2008. Nrf2 regulates the alternative first exons of CD36 in macrophages through specific antioxidant response elements. Arch. Biochem. Biophys. 477:139–145. http://dx.doi.org/10.1016/j.abb.2008.06.004.

26. Watai Y, Kobayashi A, Nagase H, Mizukami M, McEvoy J, Singer JD, Itoh K, Yamamoto M. 2007. Subcellular localization and cytoplasmic complex status of endogenous Keap1. Genes Cells 12:1163–1178. http://dx.doi.org/10.1111/j.1365-2443.2007.01118.x.

27. Yamamoto T, Suzuki T, Kobayashi A, Wakabayashi J, Maher J, Motohashi H, Yamamoto M. 2008. Physiological significance of reactive cysteine residues of Keap1 in determining Nrf2 activity. Mol. Cell. Biol. 28: 2758–2770. http://dx.doi.org/10.1128/MCB.01704-07.

28. Tanimizu N, Nishikawa M, Saito H, Tsujimura T, Miyajima A. 2003. Isolation of hepatoblasts based on the expression of Dlk/Pref-1. J. Cell Sci. 116:1775–1786. http://dx.doi.org/10.1242/jcs.00388.

29. Tanaka M, Miyajima A. 2012. Identification and isolation of adult liver stem/progenitor cells. Methods Mol. Biol. 826:25–32. http://dx.doi.org/10 .1007/978-1-61779-468-1_3.

30. Onodera K, Takahashi S, Nishimura S, Ohta J, Motohashi H, Yomogida K, Hayashi N, Engel JD, Yamamoto M. 1997. GATA-1 transcription is controlled by distinct regulatory mechanisms during primitive and definitive erythropoiesis. Proc. Natl. Acad. Sci. U. S. A. 94:4487–4492. http://dx .doi.org/10.1073/pnas.94.9.4487.

31. Tanimizu N, Miyajima A. 2004. Notch signaling controls hepatoblast differentiation by altering the expression of liver-enriched transcription factors. J. Cell Sci. 117:3165–3174. http://dx.doi.org/10.1242/jcs.01169.

32. Okabe M, Tsukahara Y, Tanaka M, Suzuki K, Saito S, Kamiya Y, Tsujimura T, Nakamura K, Miyajima A. 2009. Potential hepatic stem cells reside in EpCAM+ cells of normal and injured mouse liver. Development 136:1951–1960. http://dx.doi.org/10.1242/dev.031369.

33. Caperna TJ, Blomberg le, Garrett AWM, Talbot NC. 2011. Culture of porcine hepatocytes or bile duct epithelial cells by inductive serum-free media. In Vitro Cell Dev. Biol. Anim. 47:218–233. http://dx.doi.org/10 .1007/s11626-010-9382-3.

34. Zhang H, Liu H, Dickinson DA, Liu RM, Postlethwait EM, Laperche Y, Forman HJ. 2006. gamma-Glutamyl transpeptidase is induced by 4-hydroxynonenal via EpRE/Nrf2 signaling in rat epithelial type II cells. Free Radic. Biol. Med. 40:1281–1292. http://dx.doi.org/10.1016/j.freeradbiomed .2005.11.005.

35. Usami H, Kusano Y, Kumagai T, Osada S, Itoh K, Kobayashi A, Yamamoto M, Uchida K. 2005. Selective induction of the tumor marker glutathione S-transferase P1 by proteasome inhibitors. J. Biol. Chem. 280: 25267–25276. http://dx.doi.org/10.1074/jbc.M501014200.

36. Tee LB, Kirilak Y, Huang WH, Smith PG, Morgan RH, Yeoh GC. 1996. Dual phenotypic expression of hepatocytes and bile ductular markers in developing and preneoplastic rat liver. Carcinogenesis 17:251–259. http://dx.doi.org/10.1093/carcin/17.2.251.

37. Rada P, Rojo AI, Chowdhry S, McMahon M, Hayes JD, Cuadrado A. 2011. SCF/{beta}-TrCP promotes glycogen synthase kinase 3-dependent degradation of the Nrf2 transcription factor in a Keap1-independent manner. Mol. Cell. Biol. 31:1121–1133. http://dx.doi.org/10.1128/MCB .01204-10.

38. Chowdhry S, Zhang Y, McMahon M, Sutherland C, Cuadrado A, Hayes JD. 2013. Nrf2 is controlled by two distinct beta-TrCP recognition motifs in its Neh6 domain, one of which can be modulated by GSK-3 activity. Oncogene 32:3765–3781. http://dx.doi.org/10.1038/onc.2012.388.

39. Onoyama I, Suzuki A, Matsumoto A, Tomita K, Katagiri H, Oike Y, Nakayama K, Nakayama KI. 2011. Fbxw7 regulates lipid metabolism and

cell fate decisions in the mouse liver. J. Clin. Invest. 121:342–354. http://dx .doi.org/10.1172/JCI40725.

40. Sugimoto H, Okada K, Shoda J, Warabi E, Ishige K, Ueda T, Taguchi K, Yanagawa T, Nakahara A, Hyodo I, Ishii T, Yamamoto M. 2010. Deletion of nuclear factor-E2-related factor-2 leads to rapid onset and progression of nutritional steatohepatitis in mice. Am. J. Physiol. Gastrointest. Liver Physiol. 298:G283–G294. http://dx.doi.org/10.1152/ajpgi .00296.2009.

41. Shibata T, Kokubu A, Gotoh M, Ojima H, Ohta T, Yamamoto M, Hirohashi S. 2008. Genetic alteration of Keap1 confers constitutive Nrf2 activation and resistance to chemotherapy in gallbladder cancer. Gastroenterology 135:1358–1368. http://dx.doi.org/10.1053/j.gastro.2008.06 .082.

42. Padmanabhan B, Tong KI, Ohta T, Nakamura Y, Scharlock M, Ohtsuji M, Kang MI, Kobayashi A, Yokoyama S, Yamamoto M. 2006. Structural basis for defects of Keap1 activity provoked by its point mutations in lung cancer. Mol. Cell 21:689–700. http://dx.doi.org/10.1016/j.molcel.2006.01 .013.

43. Komatsu M, Kurokawa H, Waguri S, Taguchi K, Kobayashi A, Ichimura Y, Sou YS, Ueno I, Sakamoto A, Tong KI, Kim M, Nishito Y, Iemura S, Natsume T, Ueno T, Kominami E, Motohashi H, Tanaka K, Yamamoto M. 2010. The selective autophagy substrate p62 activates the stress responsive transcription factor Nrf2 through inactivation of Keap1. Nat. Cell Biol. 12:213–223. http://dx.doi.org/10.1038/ncb2021.

44. Ichimura Y, Waguri S, Sou YS, Kageyama S, Hasegawa J, Ishimura R, Saito T, Yang Y, Kouno T, Fukutomi T, Hoshii T, Hirao A, Takagi K, Mizushima T, Motohashi H, Lee MS, Yoshimori T, Tanaka K, Yamamoto M, Komatsu M. 2013. Phosphorylation of p62 activates the Keap1-Nrf2 pathway during selective autophagy. Mol. Cell 51:618–631. http://dx.doi.org/10.1016/j.molcel.2013.08.003.

45. Suzuki T, Shibata T, Takaya K, Shiraishi K, Kohno T, Kunitoh H, Tsuta K, Furuta K, Goto K, Hosoda F, Sakamoto H, Motohashi H, Yamamoto M. 2013. Regulatory nexus of synthesis and degradation deciphers cellular Nrf2 expression levels. Mol. Cell. Biol. 33:2402–2412. http://dx.doi.org/10 .1128/MCB.00065-13.

46. Cho HY, Jedlicka AE, Reddy SP, Kensler TW, Yamamoto M, Zhang LY, Kleeberger SR. 2002. Role of NRF2 in protection against hyperoxic lung injury in mice. Am. J. Respir. Cell Mol. Biol. 26:175–182. http://dx.doi.org /10.1165/ajrcmb.26.2.4501.

47. Wang C, Cui Y, Li C, Zhang Y, Xu S, Li X, Li H, Zhang X. 2013. Nrf2 deletion causes "benign" simple steatosis to develop into nonalcoholic steatohepatitis in mice fed a high-fat diet. Lipids Health Dis. 12:165. http://dx.doi.org/10.1186/1476-511X-12-165.

48. Kennedy AR, Pissios P, Otu H, Roberson R, Xue B, Asakura K, Furukawa N, Marino FE, Liu FF, Kahn BB, Libermann TA, Maratos-Flier E. 2007. A high-fat, ketogenic diet induces a unique metabolic state in mice. Am. J. Physiol. Endocrinol. Metab. 292:E1724–E1739. http://dx .doi.org/10.1152/ajpendo.00717.2006.

49. Zhong B, Zhou Q, Toivola DM, Tao GZ, Resurreccion EZ, Omary MB. 2004. Organ-specific stress induces mouse pancreatic keratin overexpression in association with NF-kappaB activation. J. Cell Sci. 117:1709–1719. http://dx.doi.org/10.1242/jcs.01016.

50. Takamura A, Komatsu M, Hara T, Sakamoto A, Kishi C, Waguri S, Eishi Y, Hino O, Tanaka K, Mizushima N. 2011. Autophagy-deficient mice develop multiple liver tumors. Genes Dev. 25:795–800. http://dx.doi .org/10.1101/gad.2016211.

51. Cole SE, Wiltshire T, Rue EE, Morrow D, Hieter P, Brahe C, Fisher EM, Katsanis N, Reeves RH. 1999. High-resolution comparative physical mapping of mouse chromosome 10 in the region of homology with human chromosome 21. Mamm. Genome 10:229–234. http://dx.doi.org/10 .1007/s003359900978.

52. Murakami S, Shimizu R, Romeo P-H, Yamamoto M, Motohashi H. Keap1-Nrf2 system regulates cell fate determination of hematopoietic stem cells. Genes Cells, in press.

— 98 —

Deficiency of Oncostatin M Receptor β (OSMRβ) Exacerbates High-fat Diet-induced Obesity and Related Metabolic Disorders in Mice*

Tadasuke Komori[‡], Minoru Tanaka[§], Emiko Senba[‡], Atsushi Miyajima[§], and Yoshihiro Morikawa[‡1]

From the [‡]Department of Anatomy and Neurobiology, Wakayama Medical University, Wakayama 641-8509, Japan and [§]Laboratory of Cell Growth and Differentiation, Institute of Molecular and Cellular Biosciences, The University of Tokyo, Tokyo 113-0032, Japan

Background: Obesity is associated with adipose tissue inflammation, insulin resistance, and hepatic steatosis.
Results: OSM receptor β (OSMRβ)-deficient mice fed a high-fat diet exhibited severe obesity, adipose tissue inflammation, insulin resistance, and hepatic steatosis.
Conclusion: OSM signaling has suppressive effects on the deterioration of obesity-induced metabolic disorders.
Significance: These results indicate that OSM signaling may be a promising therapeutic target of obesity-induced metabolic disorders.

Oncostatin M (OSM) belongs to the IL-6 family of cytokines and has diverse biological effects, including the modulation of inflammatory responses. In the present study we analyzed the roles of OSM signaling in obesity and related metabolic disorders. Under a high-fat diet condition, OSM receptor β subunit-deficient (OSMRβ$^{-/-}$) mice exhibited increases in body weight and food intake compared with those observed in WT mice. In addition, adipose tissue inflammation, insulin resistance, and hepatic steatosis were more severe in OSMRβ$^{-/-}$ mice than in wild-type (WT) mice. These metabolic phenotypes did not improve when OSMRβ$^{-/-}$ mice were pair-fed with WT mice, suggesting that the effects of OSM signaling on these phenotypes are independent of the increases in the body weight and food intake. In the liver of OSMRβ$^{-/-}$ mice, the insulin-induced phosphorylation of p70 S6 kinase remained intact, whereas insulin-induced FOXO1 phosphorylation was impaired. In addition, OSMRβ$^{-/-}$ mice displayed a higher expression of genes related to de novo lipogenesis in the liver than WT mice. Furthermore, treatment of genetically obese ob/ob mice with OSM improved insulin resistance, adipose tissue inflammation, and hepatic steatosis. Intraportal administration of OSM into ob/ob mice activated STAT3 and increased the expression of long-chain acyl-CoA synthetase (ACSL) 3 and ACSL5 with decreased expression of fatty acid synthase in the liver, suggesting that OSM directly induces lipolysis and suppresses lipogenesis in the liver of obese mice. These findings suggest that defects in OSM signaling promote the deterioration of high-fat diet-induced obesity and related metabolic disorders.

Obesity-induced insulin resistance is known to be a strong risk factor for the development of type 2 diabetes and subse-

quent cardiovascular disease (1). In the past decade it has been reported that obesity is underlying chronic low-grade inflammation that causes various metabolic disorders, including insulin resistance (2). Under obese conditions, a variety of inflammatory cells, including macrophages, neutrophils, T-cells, and eosinophils, are activated, stimulating infiltration, in adipose tissue (3–6). Among these inflammatory cells, classically activated macrophages (M1-type macrophages) in adipose tissue secrete proinflammatory cytokines (TNF-α and IL-1β), which induce insulin resistance (7–11). In contrast, adipose tissue in non-obese animals predominantly contains alternatively activated macrophages (M2-type macrophages) that suppress inflammation by producing anti-inflammatory cytokines, such as IL-10 (12, 13). Therefore, obesity stimulates a switch in the macrophage phenotype in adipose tissue toward the M1-type, which plays an important role in the attenuation of insulin sensitivity. However, the mechanisms underlying the development of obesity-induced adipose tissue inflammation and insulin resistance are not fully understood.

Oncostatin M (OSM)[2] is a member of the IL-6 family of cytokines, including IL-6, IL-11, leukemia inhibitory factor, ciliary neurotrophic factor, and cardiotrophin-1 (14). OSM exerts a variety of biological effects depending on the target cell by binding to the heterodimeric membrane receptor comprising the OSM specific β subunit (OSMRβ) and gp130 (15). It has been reported that OSM is produced by inflammatory cells, such as activated T cells, neutrophils, eosinophils, and macrophages (16–18), and is associated with many inflammatory diseases, including lung inflammation, rheumatoid arthritis, and multi-

---

[2] The abbreviations used are: OSM, oncostatin M; OSMRβ, OSM-specific β subunit; OSMRβ$^{-/-}$, OSMRβ-deficient; ATM, adipose tissue macrophage; AUC, areas under the curve; DIO, diet-induced obese; HFD, high-fat diet; ipGTT, intraperitoneal glucose tolerance test; ITT, insulin tolerance test; RT, room temperature; MCP-1, monocyte chemoattractant protein-1; CCR2, C-C chemokine receptor 2; TLR4, toll-like receptor 4; FAS, fatty-acid synthase; SCD-1, stearoyl CoA desaturase-1; SREBF-1, sterol regulatory-element binding transcription factor-1; PF, pair-fed; PAS, periodic acid-Schiff; SVF, stromal vascular fraction; S6K, S6 kinase.